AN EXPERIMENTAL STUDY ON

INTERFERENCE FRICTION WELDING PROCESS

A Thesis

by

DEEP KIRONONGSHU BARUA

Submitted to the Office of Graduate and Professional Studies of
Texas A&M University
in partial fulfillment of the requirements for the degree of

MASTER OF SCIENCE

Chair of Committee,	Jyhwen Wang
Committee Members,	Hong Liang Bruce Tai
Head of Department,	Andreas Polycarpou

May 2019

Major Subject: Mechanical Engineering

ABSTRACT

Friction welding is a solid state joining process in which the frictional heat and plastic deformation due to lateral force contributes to diffusion bond formed between the two workpieces in relative motion while in contact. There are several advantages that can be attributed to the friction welding processes including faster joining rates, lower heat affected zones, and refinement of material at the weld interference because of plastic deformation. Interference friction welding process is a variant of friction welding processes that has been proposed to be used to join a tube/round bar to a sheet metal/plate. The name interference friction welding refers to the fact that an interference is created between a rotating tube and the walls of the drilled hole of a stationary plate. The rotating tube is made to pass through the drilled hole of smaller diameter and hence the interference causes the plastic deformation and frictional heat due to sliding contact in axial direction (due to tube feed) and tangential direction (due to tube rotation).

In the experimental investigation, the effect of different process parameters such as feed rate, spindle speed, amount of interference, and penetration depth of the tube on the axial thrust force and the torque generated at the weld interface was studied. The change in torque and thrust force values were related to the amount of heat generation and plastic deformation at the interface that contributes to the quality of the solid state weld joint being formed.

The quality of the weld joints formed at different parameters were evaluated from the microscopic analysis and shear testing. The maximum joint strength observed was 62 MPa which was 33 % of the yield strength of the Al 6061 material.

Moreover, the joint strengths were compared with the interference fit joints that were formed from the shrink fitting operation. The shear strength of the shrink joint was obtained to be 10.89 MPa. In addition, an analytical model has been proposed based on the existing literature on friction welding processes. It is shown that the model can accurately predict the thrust force and torque values during the interference friction welding process for the given experimental parameters.

DEDICATION

I would like to dedicate all of my efforts towards this thesis to my parents and friends. My parents have always believed in me and motivated me to aim high and work to reach beyond my potential. My friends have been my family away from my home and provided a vital support to keep up the spirit high during the crucial times.

ACKNOWLEDGEMENTS

As it is rightly quoted “Persistence is the key that will open up any door that has been closed by resistance” -John Dilemme. During the course of my research study there have been several hindrances that offered resistance in moving forward. I could overcome all the resistances with patience and persistence only because of the optimism and motivation provided by Dr. Wang, who always inspired me to focus on the next step after eliminating smaller roadblocks.

I would also like to thank my committee members Dr. Tai and Dr. Liang who were always willing to provide guidance whenever needed. In addition, I would also like to thank Dr. Hung for giving me the permissions needed for training to comply safety norms of the department and lending me the IR temperature gun and the tachometer.

I would like to extend my deep sense of gratitude to Mr. Adam Farmer for training me to use the machines. I am highly obliged to my lab colleague, Shengwei Chen who was always available to help me when I encountered any problem with Abaqus. I would like to express my sincere gratitude to my peers Shyam Sunder Balasubramanian and Jyoti Sharma, who were always willing to offer help and provided me the motivation and support needed at various stages of my graduate curriculum. I am also thankful to the High Performance Research Computing team for their supercomputing facility and the MMET and Mechanical engineering department for their excellent facilities. Finally, I would like to express my utmost gratitude to my parents for their constant encouragement and moral support.

CONTRIBUTORS AND FUNDING SOURCES

This work was funded and supervised by Dr. Jyhwen Wang's research group. All the work for the thesis was completed by the student independently.

NOMENCLATURE

FSW	Friction Stir Welding
FHPP	Friction Hydro pillar processing
FWTPET	Friction Welding process of Tube to Plate using an External Tool
t	Time
CNC	Computer Numerical Control
LED	Light Emitting Diode
LC	Least Count
I/D	Inside Diameter
O/D	Outside Diameter

TABLE OF CONTENTS

Page

LIST OF FIGURES

Page

LIST OF TABLES

Page

1 INTRODUCTION: MECHANISM FOR OBTAINING SOLID STATE JOINT

Interference Friction Welding is a novel solid state pressure welding concept in which there is an establishment of an atom-atom bond between the two pieces to be joined through intimate contact between oxide free areas achieved under pressure created as a result of interference between the mating surfaces and without the formation of liquid phase.

This process offers a brighter prospective as it has all the advantages of solid state welding processes like lower heat affected zone around the welding area, better dimension control with lower distortion, no weld porosities or hot cracking, no requirement of filler metal or welding equipment and several other advantages as compared to fusion welding process. In addition, welding of Aluminum by fusion welding process has always been a challenge due to oxide layer formation which can be overcome by using AC power source or reverse polarity. However while welding, Aluminum can readily react with filler metal, which can lead to hot cracking, breaking and brittle metal that can break later on.

In this study, the mechanism of solid state bond formation between a rotating tube and a stationary plate with drilled hole is studied. The required contact pressure is achieved by creating an interference between the rotating tube and the drilled hole. Heat generation occurs as a result of excessive plastic deformation and frictional sliding. Mohamed and Washburn et al. [1] performed experimental study to check the role of oxide film in friction welding. They observed that in order to initiate welding this film has to be broken and

plastic flow of the metal is a pre requisite for oxide breakage. In order to create the solid state bond, surface films have to be removed or reduced in amount.

Surface films fall into two categories:

- Oxide film: All metals except gold possess an oxide film at room temperature. In most of the metals the oxide film reaches a limiting thickness in the range of 20-100 angstroms at room temperature.[2]
- Contaminant film: This film consists of moisture and greases. Suitable techniques which are successful in reducing these films are a combination of chemical and mechanical cleaning [3]

There are mainly two theories that explain the mechanism of formation of solid state bond by pressure welding which have been discussed in this section.

1.1 Film Theory

This theory presents that if two clean surfaces are brought into intimate contact, a weld will be created. This theory considers the different weldability of various metals to the relative hardness of the bulk parent material and oxide. Initiation of welding is controlled by the degree of fragmentation of the oxide film. However, Mohamed et. al. [1] studied that the oxide films crack at deformations much less than the minimum welding deformation. This means that there is a minimum energy level that needs to be overcome to obtain a weld after the oxide film cracks.

1.2 Energy Barrier Theory

The energy barrier theory suggests that even if clean surfaces are brought into contact, no weld will result until the minimum required energy barrier is overcome. Parks et. al. [1] proposed the barrier to be recrystallization whereas Erdmann-Jesnitzer et.al. [1] suggested it be diffusion. Semenov et. al. [1] suggested that the energy barrier is due to the misorientation of the crystals at the contact surface, as he could weld aluminum, copper and silver at the temperature of liquid nitrogen. It is not justifiable to assume that welding at this temperature occurred due to diffusion or recrystallization. McEwen and Milner et al. [4] have presented that immiscible metal pairs can be joined satisfactorily.

The current research study involves the investigation of the interference friction welding process for joining a tube and a stationary sheet metal plate.

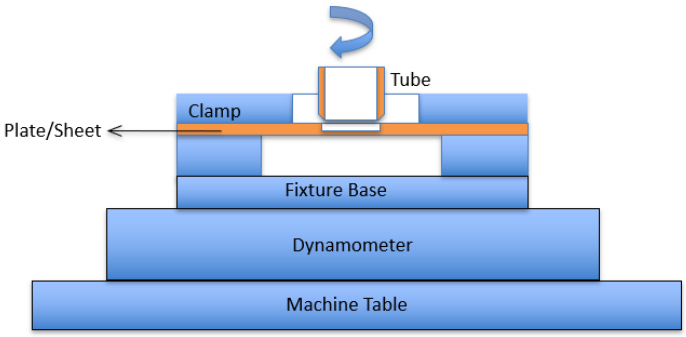

Figure 1 Schematic diagram of the experimental setup

Figure 1 depicts the schematic of the interference friction welding process where the sheet metal is clamped into the fixture mounted on a dynamometer installed with strain gauges which senses the thrust force and torque generated at the interface. The dynamometer is mounted on the machine table. The tube is mounted on the machine

spindle, rotated at a high rpm and fed through the sheet metal plate causing heat generation due to frictional sliding and plastic deformation. This heat generation leads to formation of solid state joint formation between the tube and the sheet metal plate.

Friction welding has been widely used over several decades. Chapter 2 describes about the existing friction welding processes, developmental work in the domain, similarities and differences with the proposed process under study.

The details about all the components required to perform the interference friction welding experimental analysis successfully, including the testing apparatus and the machine requirements has been discussed in Chapter 3 of this thesis.

The experimental procedure for proposed interference friction welding process, the observations during the study, parametric analysis of the process, shear testing procedure and results, microscopic analysis results, analysis of shrink fitting joints has been presented in Chapter 4 of this thesis.

The analytical model that can be applied to the process under study has been discussed in Chapter 5 of this thesis. The results of the analytical model and comparison with the results obtained from the experimental analysis has also been presented.

A summary of observations and outcomes from this experimental study on interference friction welding process has been discussed in Chapter 6 of this thesis, along with the potential future work that can be done to optimize the process and use the process for versatile applications.

2 BACKGROUND AND LITERATURE REVIEW

2.1 Existing solid state joining processes and their applications

The process under study, of joining a rotating tube and a plate by creating an interference is comparable to similar widely used process applications of friction welding like Friction Plug Welding also known as Friction Hydro Pillar Processing (FHPP) and Friction Stir Welding (FSW). However, the joint configuration for the process in this study is different as no separate tool is needed and the contact interface between the drilled hole and the rotating tube is not taper as in case of FHPP. In addition since the current process is applicable for sheet metal workpieces unlike FHPP which has been used for thick walled applications, the hole formation process also differs in the present study.

Moreover, in Friction Stir Welding the tool causes the stationary work pieces to join by the heat generation due to the interaction between the tool pin and tool shoulder with the stationary work piece whereas in the current process under study, the tube itself participates in the welding process.

The source of the heat generation for interference friction welding under the current study is the frictional sliding between the cylindrical surfaces of the rotating tube and the walls of the drilled/punched hole in the stationary plate and plastic deformation of the tube and the plate material due to the interference created between the mating surfaces. The goal is to obtain a solid state diffusion joint between the tube and the sheet metal work piece. The material for the tube and sheet metal used in this research is Al 6061. The composition of the material has been discussed in the next chapter.

Friction Stir Welding and Friction Plug Welding are established processes widely used and lot of work has been done in the field to understand the concept and mechanism of friction welding processes. Though the joint interface is different, certain useful results of Friction Plug Welding and Friction Stir Welding can be applied to the current process under study. Friction Stir Welding is a relatively new metal joining process in which a tool comprising of a pin projecting out of a shoulder is rotated at a high speed and fed between the two workpieces that are to be joined. Figure 2 depicts the typical FSW process and the tool as presented by Kumar et. al. [5] in their research study.

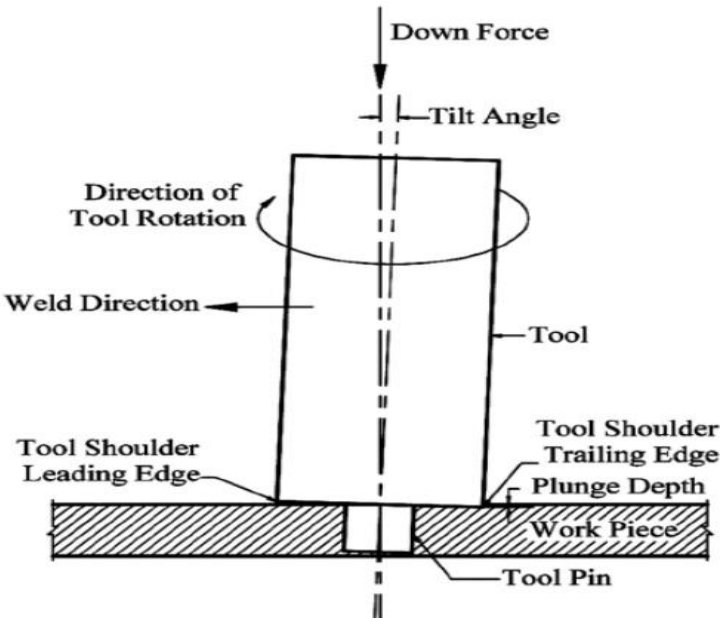

Figure 2 Schematic diagram of a typical FSW process and tool (reprinted) [5]

The stirring action between the work pieces, the tool shoulder and pin causes sufficient amount of heat generation which causes the material of the work pieces to soften and plasticize resulting in joining of the work pieces without melting of the material.

Initially, Friction Stir Welding process was used for the joining of aluminum and its alloys because of limitations of the traditional fusion welding processes for those alloys with high thermal expansion coefficient, high thermal conductivity and high electrical conductivity as claimed by Sattari,et al. [6]. Since then Friction Stir Welding process is also used to join metals including copper, steels and titanium in similar and dissimilar combinations, and other materials including plastics, composites and wood. (Keydon and Veeredhi , 2016) [7].

2.2 Developmental work in friction welding processes

Till date, a lot of research has been done on tools, materials and process optimization contributing to significant advancement of the FSW process. Micro Friction welding is a variant of FSW for joining of materials of thickness 1 mm or less. Butt and lap joint configurations have been tried out using Micro Friction Stir Welding process (Ahmed, et al., 2014) [8]. Nishihara et al. performed initial feasibility studies on Micro Friction Stir Welding process for AZ31 magnesium alloys (Nishibara & Nagasana, 2004) [9] and later Scialpia et al. [10, 11] focused on mechanical properties of micro friction welded joints of 2024-T3 alloy with 6082-T6 alloy and observed that the alloys were successfully joined and the joint strength was close the strength of the weaker 6082-T6 base metal alloy. Keydon and Veeredhi [7] in their discussion mention about three zones namely the Stir Zone (SZ), the thermo-mechanically affected zone (TMAZ) and the heat affected zone (HAZ).

The tool pin configuration for FSW process is not applicable in the current interference friction welding process under study. The Friction Plug Welding process

seems more comparable to current process under study with difference being the usage of taper plug in place of the straight tube specimen itself and the hole making process in the stationary specimen. However, this has a major influence on the material interaction and the heat generation at the interface as it is easier to obtain higher contact pressures and material interaction with taper surfaces. Moreover the feasibility of joining tube/bar to a thin sheet has not been evaluated till the present study. Figure 3 shows three sequential stages of Friction Plug Welding process. The conical rotating element shown in Figure 3 is the stud, which itself is the tool for Friction Plug Welding Process.

The process starts with a dwell stage as an external rotating stud is pressed into a crack-hole, which is pre-machined to fully open the existing crack, leading to frictional heating along the stud–hole interface.

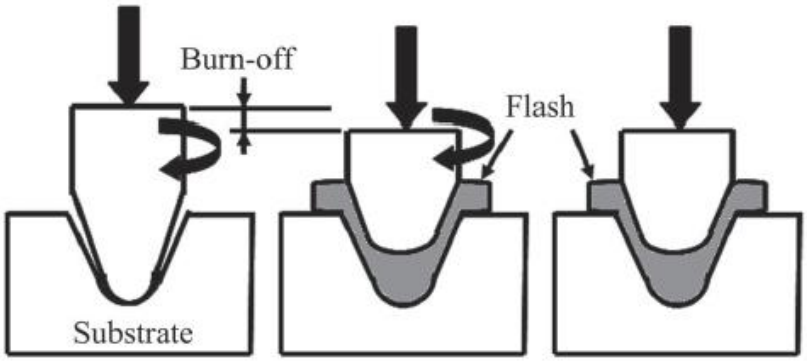

Figure 3 Schematic diagram showing (a) dwell stage, (b) burn off stage and (c) forging stage of the Friction Plug Welding process (reprinted) [12]

Next, the rotating stud is forced into the crack-hole resulting in plastic flow of stud material through the stud–hole clearance depicted as flash in the Figure 3, which is referred to as the burn off stage. As the crack-hole is completely filled up by the flash which acts as a filler material, the rotational motion of the stud is stopped and the force is increased

to promote a solid-state bond between the stud and substrate that is defined as the forging stage.

Amitava et. al. [12] performed a coupled experimental and numerical study on FHPP of ASTM A36 steel to understand the effect of processing conditions on the joint structure and properties. An axis-symmetric heat transfer analysis was carried out to compute the temperature field. A transient heat transfer analysis was conducted considering the governing equation in two-dimensional cylindrical co-ordinate system as,

$$\frac{1}{r}\frac{\partial}{\partial r}\left(kr\frac{\partial T}{\partial r}\right)+\frac{\partial}{\partial z}\left(k\frac{\partial T}{\partial Z}\right)+\dot{Q}=\rho\ C_p\frac{\partial T}{\partial t} \quad (1)$$

where, k, ρ, $C_{p,}$ T, t, r and z referred to the thermal conductivity, density, specific heat, and temperature, time variable, radial distance from the central stud axis, and position coordinate in axial direction respectively. The term $\dot{Q}$ represents the heat transfer along the stud hole interface which can be expressed as,

$$\dot{Q} = \eta_h[\eta_m(1-\delta)\tau_y + \delta\mu_f P_N](\omega r_1)(\frac{A_i}{V_i}) \quad (2)$$

where η_h is the fraction of total heat transferred to stud, η_m is the fraction of mechanical work due to sticking friction converted to heat, r_1 is the radial distance from the stud axis, ω is the angular speed of stud, P_N is axial pressure on the stud, τ_y is temperature-dependent shear yield stress of stud material, δ is the amount of slip, and μ_f is the effective coefficient of friction. The value of η_h was assumed to be 0.5 considering the equal partitioning of the heat generated along the stud-substrate interface as both the mating surfaces are of the same material. The value of η_m was considered to be 0.4 as it provided the best match between the computed and the measured values of thermal cycles

for all cases. A_i and V_i represented the contact surface area and the volume of the element associated with the interface.

The local variations in fractional sliding (δ) and co-efficient of friction (μf) were considered as,

$$\delta = -0.026 + 0.275\exp(r_1 \frac{\omega}{1.87}) \quad (3)$$

$$\mu_f = 0.5 \exp(-\delta r_1 \omega) \quad (4)$$

The computed thermal cycles were used to estimate the hardness distribution across the joint. For any solid state joining process, coefficient of friction between the mating surfaces is of vital importance as it has a dominant effect on the frictional heat generation.

Srivatsan et al. [13] studied the interaction between the Friction Stir Welding tool and base metal at different contact pressures (13 MPa, 26 MPa and 39 MPa) and rotational speeds (200 rpm, 600 rpm, 1000 rpm, and 1400 rpm) experimentally and determined the coefficient of friction for different set of parameters. The coefficient of friction was observed to vary in the range of 0.15 to 1.4 and maximum temperature was observed to be 450 ºC. It was observed that the coefficient of friction increased with the increase in the temperature. A steep increase in temperature was observed after the temperature increased beyond a specific critical temperature . The critical temperature decreased from 250 C at a contact pressure of 26 MPa to 200 C at a contact pressure of 39 MPa as indicated in Figure 4.

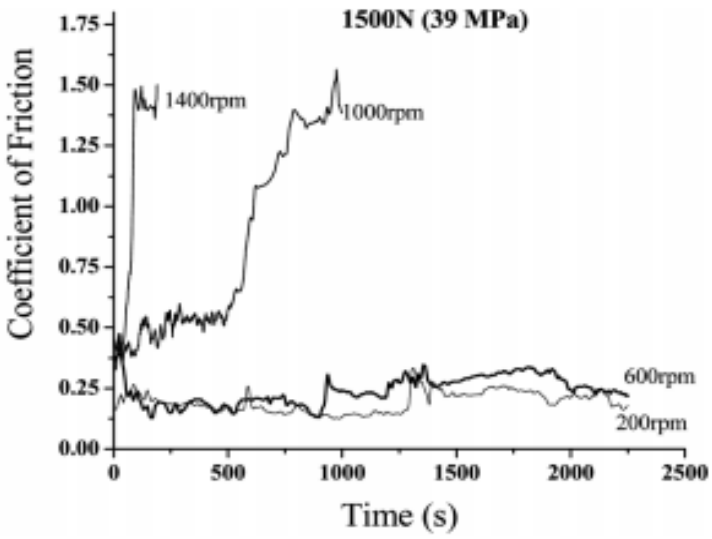

Figure 4 Coefficient of friction for different spindle speeds [13]

At a specific contact pressure below the critical temperature, the maximum coefficient of friction was observed to be 0.6 and above the critical temperature it reached a value as high as 1.4. The steep increase in the coefficient of friction was observed to be due to the seizure phenomenon and the sticking contact condition between the tool and the work piece.

A.C Nunes, Jr. et al. [14] developed an analytical model for the mechanics of Friction Plug Welding. The model accounted for coupling of plastic deformation that is due to the material flow and thermal response because of plastic heating. The predictions of the analytical model were compared with the experimental results and were found to be close enough.

There have been several studies about joining a tube to a plate similar to the goal of this research study however the approach used has been similar to Friction Stir Welding

using an external tool. Kumaran, S. Senthil et al. [15] and Muthukumaran et. al. [16] performed experimental analysis on friction welding process of tube to tube plate using an external tool in with hole and without hole (FWTPET). Figure 5 depicts the schematic of the experimental setup of the FWTPET process.

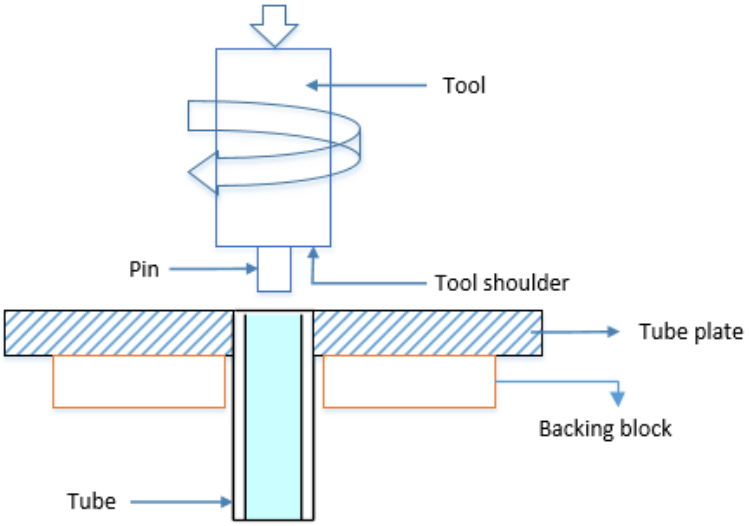

Figure 5 FWTPET setup [16]

The prerequisite to achieve a FWTPET weld are temperature & pressure which should be high enough for forging. The tool used in the study was made up of tool steel material. The tube plate used for the study was of AL2025 material and the tube was commercially available Al 6061 tube. The AL2015 was cut into the size of 50 mm × 50 mm using shearing machine. The tube outer diameter was 18.8 mm and the inner diameter was 14.8 mm. The tubes were cut into various lengths of 26 mm, 27 mm and 28 mm and each of the 3 pieces were with hole and without hole respectively as shown in Figure 6.

Figure 6 Tube With/Without hole (reprinted) [15]

The holes of 2 mm diameter were drilled on the tube outer surface. Further, depending on the diameter of the tube a hole at the centre of the plate was drilled. A backing block was used for ensuring defect free joints with higher strength and lower distortion. The assembly of the work piece along with backblock fixture was clamped on to the machine table and the tool was fixed to the tool holder of the machine. Heat generation occurred when the rotating tool and the tool shoulder came in contact with the stationary workpiece. When the plate material reached plastic condition, the plastic flow of metal occurred towards the center of the tool axis and penetrated through the holes in the tube and occupied the gap. The pin acted as an anvil and forged the metal to plastic condition. Hence, the enormous pressure and high temperature was achieved between the tube and tube plate interface and a metallurgical bond was created. The joints formed by this process have been shown in Figure 7.

Figure 7 Joints from FWTPET process (reprinted) [15]

The joints strength were analyzed by compression test performed on Universal Testing Machine. It was also observed that tool with hole process was better than the tool without hole process. The joint strength for with and without hole joint improved with increase in spindle speed. The joint strength of plate to tube without hole at 1500 rpm was observed to be 114 MPa and tube with hole it and plate was observed to be 166 MPa. Taguchi approach was applied to predict the most influential control factors which would yield better joint strength. The most influential process parameter was determined using statistical analysis of variance (ANOVA) and comparative analysis of effect of external tool being with hole and without hole was made. It was observed that the tool rotational speed was the most influential process parameter followed by pin depth and tool projection.

A similar study was performed by Kumaran, S. Senthil et al. to analyze the effect of tube projection into the plate. The parent metals employed in this study were commercially pure aluminium plate and SA106 Gr.B Steel Tube. The experiment was performed using 6 mm rolled plates of commercially pure aluminium and cut into the

predetermined sizes (50 mm x 70 mm) by means of a power hacksaw. Likewise, steel tubes of 19 mm external diameters were cut into required size (40 mm height). Further, the tubes were fixed in their respective holes with 2 mm depth (without tube projection) and steel tube with 2 mm projection in tube plate. The machine and rest of the experimental setup and procedure was same as discussed before by same authors for analysing the influence of the hole in the tube. However, the tool used in the study was of tungsten alloy material. The joint strength of steel tube with projection through the aluminium plate was tested to be 70.45 MPa and joint strength of steel tube without projection was tested to be 67.93 MPa. Hence, the joint strength of steel tube with projection in the Aluminium plate was better than the steel tube without projection.

S.Muthukumaran et al. [16] studied the bonding interface microstructure and mechanical properties of the steel tube welded to aluminum plate by FWTPET (Friction welding of tube process). Metallurgical bonding between tube and tube plate was studied using a micrograph. The tubes without and with projection into the tube plate were investigated with micro structural analysis as depicted in Figure 8(a), 8(b) and Figure 9(a), 9(b) respectively. It was observed that grain refinement occurs at the bond interface which led to high joint strength and hardness. The interface of the sample welded with tube projection was found better in the micrograph with lesser discontinuities than the sample welded without the projection. Formation of continuous layer at interface leads to better bonding of dissimilar metals. The micro hardness plot revealed that hardness at the interface was slightly higher in the sample welded with 2 mm tube projection (98.6 Hv) when compared to the sample welded without tube projection (55 Hv).

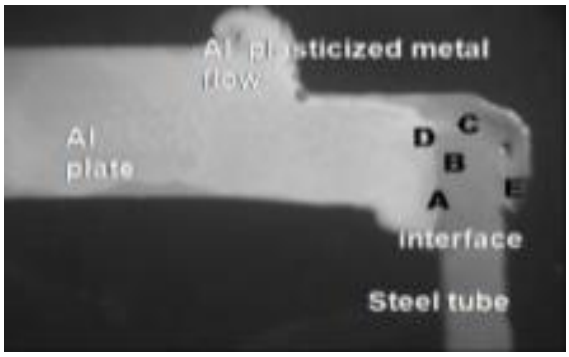

(a)

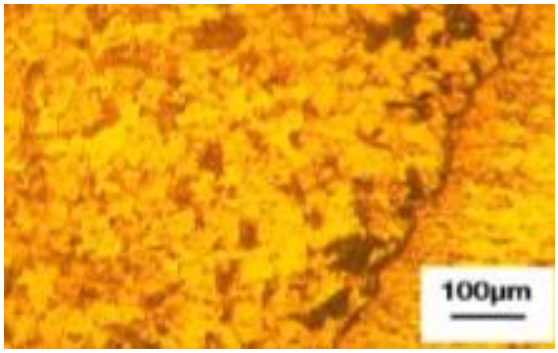

(b)

Figure 8 (a), (b) Microstructure of sample welded without tube projection (reprinted) [16]

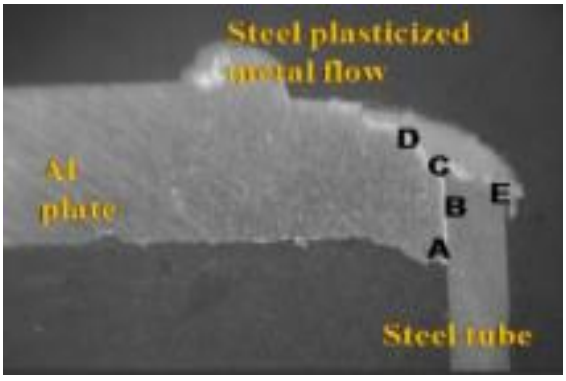

(a)

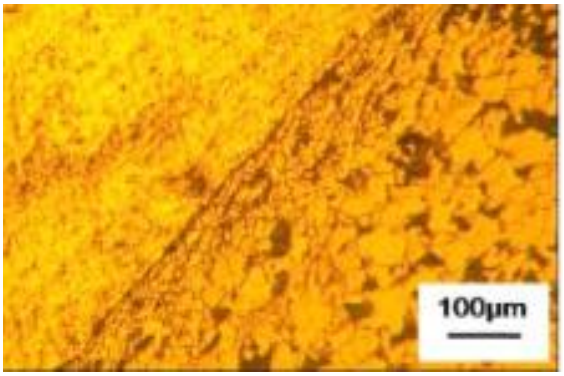

(b)

Figure 9 (a), (b) Microstructure of welded sample with tube projection (reprinted) [16]

Miller et al. investigated the 3D finite element modeling of friction drilling process referencing Friction Stir Welding process using ABAQUS Explicit model. The validation was made by comparing the thrust forces and torques of finite element modeling results to experimental measurements and analytical model [17].

3 EXPERIMENTAL SETUP

Interference welding offers a novel technique of obtaining solid state joints between a tube and a plate which otherwise is difficult to join by fusion welding process because of excessive distortion, joint configuration and oxide layer formation in Aluminum. The current study aims to investigate the feasibility of obtaining a solid state interference joint between a rotating tube and a stationary plate by establishing experimental parameters that would experimentally lead to consistent formation of a solid state diffusion bond having considerably higher joint strength as compared to shrink fit or interference force fit joints and comparable joint strengths to fusion welded joints with added on advantages.

The foremost aim of the research study is to experimentally analyze the torque and thrust force generated at the interference during the interference friction welding process corresponding to different set of process parameters like spindle speed, feed rate of the rotating tube, amount of interference between the tube and the drilled hole in the stationary plate, and thickness of the plate. Based on the measured thrust force and the torque values, it can be decided whether a typical milling machine or a lathe can be used for the intended process presented. The formation of the diffusion bond between the mating surfaces is verified by microscopic analysis of the cross section of the interface. In addition, the strength of the joint is evaluated by performing a shear test of the joint using a United Tensile testing machine.

This chapter describes the apparatus used to perform experiments on interference friction weld joints and to record the parameters like force and torque for further analysis of the experimental results.

3.1 Introduction

The apparatus includes three-axis computer numerical control (CNC) milling machine, drill bits for aluminum and low carbon steel material, fixture for holding the plate with drilled hole, aluminum and low carbon steel tubes and round bars, and the data acquisition system for recording the force and torque data during the experiment. In addition, tachometer and infrared non-contact type digital thermometer is used to record the number of rotations of the spindle and the material temperature near the interfering region. Further, there are several components in the data acquisition system that allow us to record the force and torque data during the course of experiment which are also discussed in this section.

3.2 Machine Selection

The machine selected for the interference friction welding experiment is the Bridgeport three-axis computer numerical control (CNC) milling machine. The CNC milling machine has the capability of 4000 rpm maximum spindle speed about z-axis which is appropriate for the application of this experiment. In order to achieve uniform interference between the tube and the drilled hole, it becomes extremely important that the machine spindle spins true to the spindle axis. The run-out error of the machine should be as small as possible. The run-out error of the machine was checked using the dial gauge and calibration pin gauges as shown in Figure 10. The dial gauge with a magnetic base

was placed on the machined face of the machine table. The error close to the spindle using a pin gauge was observed to be 0.0889 mm (0.0035in).

The error was a cumulative effect of run-out errors between the machine spindle and tool holder and the tool holder and the gage pin.

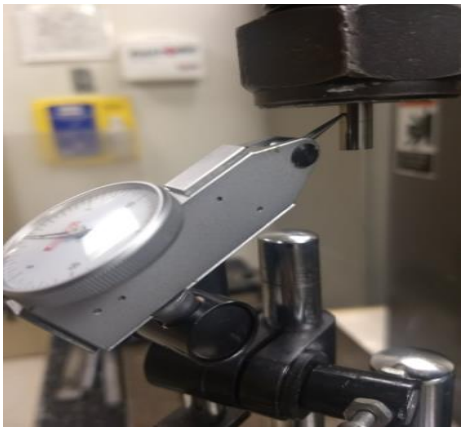

Figure 10 Run-out error measurement of machine spindle with a dial gauge

3.3 Workpiece/Specimen Preparation

In order to achieve the required interference between the mating surfaces of the rotating tube and the drilled hole, dimensional and geometric accuracy of the drilled hole and the tube becomes critical. Al 6061-T6 tubes of 12.7 mm (0.5 inch) outside diameter and 2.1082 mm (0.083 inch) wall thickness and aluminum plate of 304.8 mm ×304.8 mm (12 inch ×12 inch) were procured. The plate size was reduced to 200 mm ×100 mm using a band saw in order to rigidly clamp the plate by the clamping plate of the fixture. Depending on the amount of interference required, corresponding size of a twist drill bit was used. Based on the penetration of the tube desired for a given trial of an experiment, the tube of given length was cut using a handsaw. The material composition and the

mechanical properties of the Al 6061 material provided by the manufacturer have been listed in the Table 1 and Table 2 respectively.

Element	Percentage
Al	Remainder
Cr	0.04 - 0.35
Cu	0.15 - 0.4
Fe	0.7 max
Mg	0.8 - 1.2
Mn	0.15 max
Si	0.4 - 0.8
Ti	0.15 max
Zn	0.25 max

Table 1 Material composition of Al 6061-T6 for the Tube and sheet metal plate [37]

Property	Value
Elongation % in 50.8 mm	12
Modulus of Elasticity (MPa)	68947.6
Ultimate shear strength (MPa)	186.15
Yield Strength (MPa)	255.106
Ultimate strength (MPa)	289.57

Table 2 Mechanical Properties of the Al 6061-T6 material [37]

3.4 Workpiece holding fixture

The workpiece holding fixture was designed and fabricated to hold the plate specimen rigidly throughout the drilling and interference friction welding experiment. The uniformity and consistency of interference throughout the circumference of the joint has a major effect on the quality of the joint. Hence it becomes critical to secure the plate rigidly to avoid any sideways movement of the stationary clamped plate during the entire experiment. The fixture used was of similar design as used by Nair et. al. in his research experiments on incremental sheet forming. The base of the fixture was mounted on to the

table mounted dynamometer using bolts and was fabricated to be of same length and width as that of the top surface of the dynamometer. The thickness of the base was 20 mm so that it can endure the vertical z forces generated during the interference friction welding experiment. The order to provide modularity to the fixture, the frame of the fixture was formed by bolting together 4 individual rectangular bars of 50 mm height and 20 mm thickness using 9.525 mm bolts. Two of the bars were of 200 mm length, same as the width of the dynamometer and the base plate and two of them were of 100 mm length altogether forming a rectangular frame on which the specimen plate is secured. In order to clamp the specimen plate, threaded holes on the four vertical bars are drilled and a clamping plate of size 200 mm×140 mm with an internal rectangular cut out of 100 mm×75 mm at the center of the plate was used. The clamping plate was bolted on top of the specimen plate to securely clamp the specimen plate.

The experimental fixture can be better understood looking at Figure 11, displaying the fixture bolted on the table mounted dynamometer.

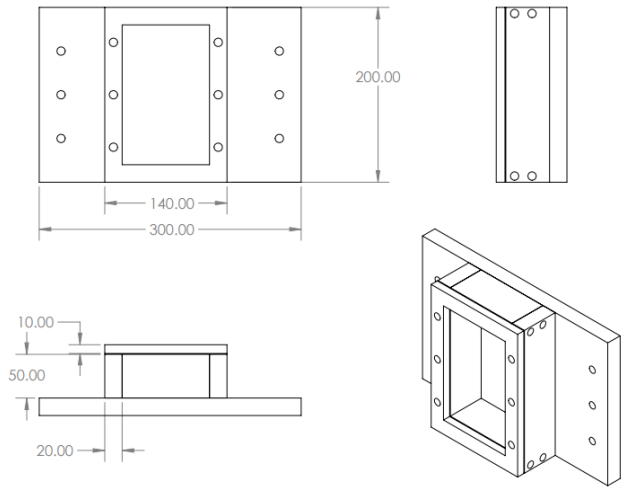

Figure 11 2-D views and isometric view of the fixture

3.5 Data Acquisition system components

In order to establish the parameters for the interference friction welding, accurately recording the data for post experimental analysis is of prime importance. The table mounted three axis dynamometer serves as the major component of the data acquisition system. It is mounted on the table of the Bridgeport CNC milling machine. The fixture that holds the sheet metal specimen is bolted on the top of dynamometer. The forces and the torque acting on the sheet metal workpiece are sensed by the dynamometer and converted to corresponding voltage signals. These voltage signals are then fed to the amplifier connected to the dynamometer. The amplifier amplifies the weaker signals and the stronger signals from the output of the amplifier are fed into the analog to digital converter. The output in form of digital signals is captured by the Lab view data acquisition software installed in the computer.

3.5.1 Dynamometer

The dynamometer measures the forces in the three principal directions and the torque along the z direction. The signals from the dynamometer are amplified by connecting the dynamometer to an amplifier which amplifies the weak voltage signals from the dynamometer. The dynamometer used in the experiment was MC 818 series table mount type dynamometer manufactured by Advanced Mechanical Technology Inc. (AMTI) as shown in Figure 12. The dynamometer has 4 channels to measure the force along x, y, z directions and the moment along x direction. The dynamometer generates analog signals corresponding to the force sensed. The force measurements are done using strain gauges integral to the dynamometer.

Figure 12 Fixture fastened to table mounted dynamometer

3.5.2 Amplifier

The sensitivity of the dynamometer is of the order of microvolts/volt/unit load. Thus, the Missile command amplifier as shown in Figure 13 is connected to amplify the weaker signals coming from the output of AMTI'S dynamometer. The amplifier requires a 115 volts AC, 50-60 Hz power supply input. The voltage gain can be adjusted using switches provided on the panel. The voltage gain for the experiments was 4000. The amplifier's output cable comprised of 9 different wires of different colors. Four wires corresponded to the force measurements along three orthogonal directions and moment along x axis. The rest of the five wires were grounded. To ensure safety, one of the ground wires was connected to the body of the amplifier.

Prior to the start of experiment the amplifier channels were balanced. Each channel had a pair of LED lights which when lit up indicated that the particular channel was unbalanced which could result into positive or negative error in the results depending on which LED light was lit.

Figure 13 AMTI amplifier

In order to balance the amplifier channels, the potentiometers in every channel were balanced which was indicated by the switching off of both the LED lights. In order to ensure accurate results, the balancing was performed after 30 minutes of warm up time for the amplifier.

3.5.3 Analog to digital converter

The output analog signals from the amplifiers are fed into the analog to digital converter to feed the signals to the data acquisition software. The converter used in this study had maximum operating voltage range of +/-10 volts and was of model USB-6009 by National Instruments.

The wires coming from the amplifier carrying analog signals were connected to the analog side of the converter using a differential method. The value that enters the converter is the difference between the positive and negative terminals to which the wires coming in are fed. Figure 14 shows the incoming wires from the amplifier connected to the analog to digital converter.

Figure 14 Analog to digital converter

The wire carrying the signal for force measured in z direction was fed into port number 8 on the analog side of the converter which acts as a positive terminal of the differential connection. A ground wire was connected to port 9 which acts as a negative terminal and hence completes the connection. In the same manner, the wire carrying the torque measured at the interface was fed to port 11 of the analog side of the converter and ground wire was connected to port 12. The output of the digital side of the converter is connected to the data acquisition software installed in the computer using a USB wire.

3.5.4 Data acquisition software

Data acquisition software receives the data in digital form from the analog to digital converter and processes the data for further analysis. The data acquisition software used for acquiring data was LabVIEW Signal Express LE. The data sampling rate was set to be 500 Hz meaning that 500 data points were recorded in one second. The data further can be converted to different file formats and processed further for representation.

3.6 Calibration of data acquisition system for measurement of thrust force

The thrust force generated in axial direction during the interference friction welding process is sensed by the strain gauges in the dynamometer and corresponding voltage signals for axial force are generated.

In order to calibrate the dynamometer for z-force measurement, standard set of dead weights were placed on the table mounted dynamometer as shown in Figure 15.

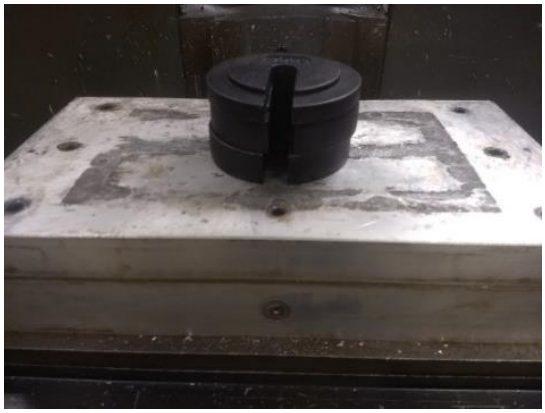

Figure 15 Calibration of thrust force

The voltage signals for 1 kg, 3 kg, 4 kg, 5 kg, 6 kg, 7 kg, and 8 kg standard weights were recorded and the linear relationship between the voltage and the axial force along z-direction was observed. The recorded values have been listed in Table 3 below.

Load (kg)	Axial Thrust Force (N)	Voltage (volts)
1	9.81	0.064
3	29.43	0.096
4	39.24	0.113
5	49.05	0.129
6	58.86	0.146
7	68.67	0.163
8	78.48	0.179

Table 3 Recorded voltage values for standard dead weights

Using this relationship depicted in Figure 16, a correlation was established which was utilized to convert the recorded voltage signals in volts corresponding to the forces generated during the experimental trials to forces in Newton.

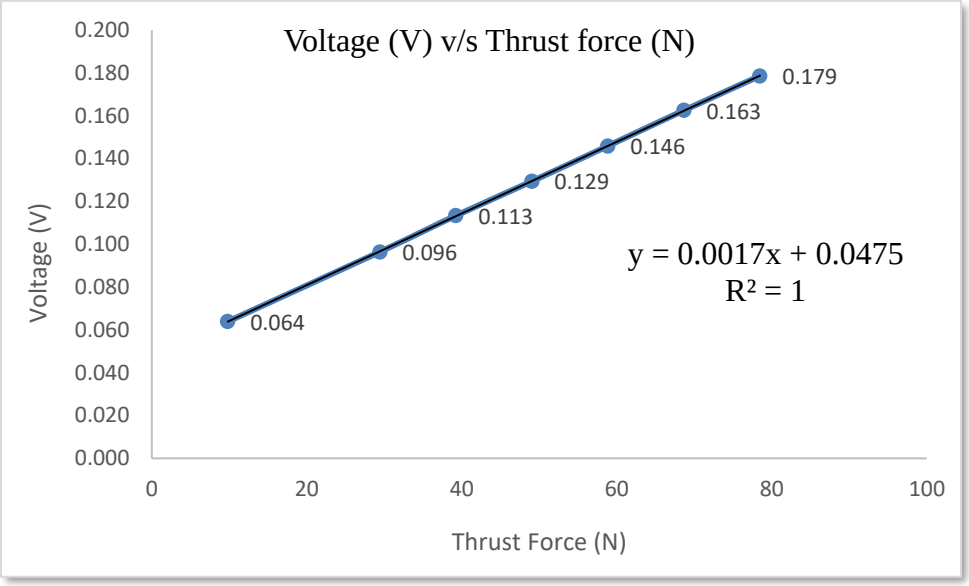

Figure 16 Relationship between recorded voltage signals and corresponding applied thrust force (N)

3.7 Calibration of data acquisition system for measurement of Torque

The torque generated at the interface of the two mating surfaces during interference friction welding process is sensed by the strain gauges in the dynamometer and corresponding voltage signals are generated.

In order to calibrate the dynamometer for torque measurement, a known amount of torque was applied to one of the bolts of the fixture using a TEKTON make 1/2" Drive Click Torque Wrench as shown in Figure 17. The voltage readings were recorded for

torque wrench scale set to 13.6 Nm, 27.1 Nm, and 40.7 Nm and the procedure was repeated thrice at each value of torque.

Figure 17 Torque applied to Fixture bolts

The torque wrench was calibrated using a 1/2" Drive Digital Torque Wrench Adapter Tool shown in Figure 18. The accuracy of the digital torque wrench adapter tool was $\pm$2 % with ½ inches drive.

Figure 18 Digital Torque Wrench Adapter

Torque (Nm)	Voltage (V)
13.6	1.240
27.1	1.702
40.7	2.650

Table 4 Average torque values recorded for 3 different torques

From this calibration process, the values listed in Table 4 were obtained. Based on these values a relationship between the recorded voltage signals and the torque values in Nm was established as shown in Figure 19 and later used in analyzing the recorded values of torque during the interference friction welding experiment.

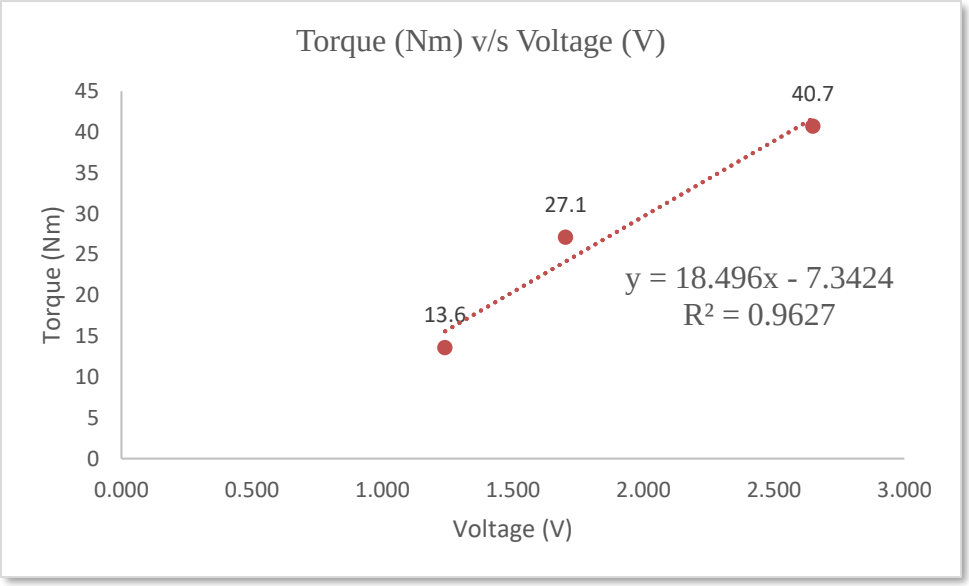

Figure 19 Relationship between recorded signals and corresponding applied torque (Nm)

3.8 Signal collection and signal processing using LabVIEW

The digital signals coming from the analog to digital converter are processed by the LABVIEW (2016 version) software. The DAQ assistant creates, edits and runs tasks using NI-DAQmx.

The continuous sampling of the data points at the rate of 500 Hz was selected. The data recording and storage at the set frequency was made possible by using a while loop that stores the data for given number iterations. The block diagram as shown in Figure 20 was created within the while loop to fetch the required force and torque data in form of array and export the array in form of an excel document.

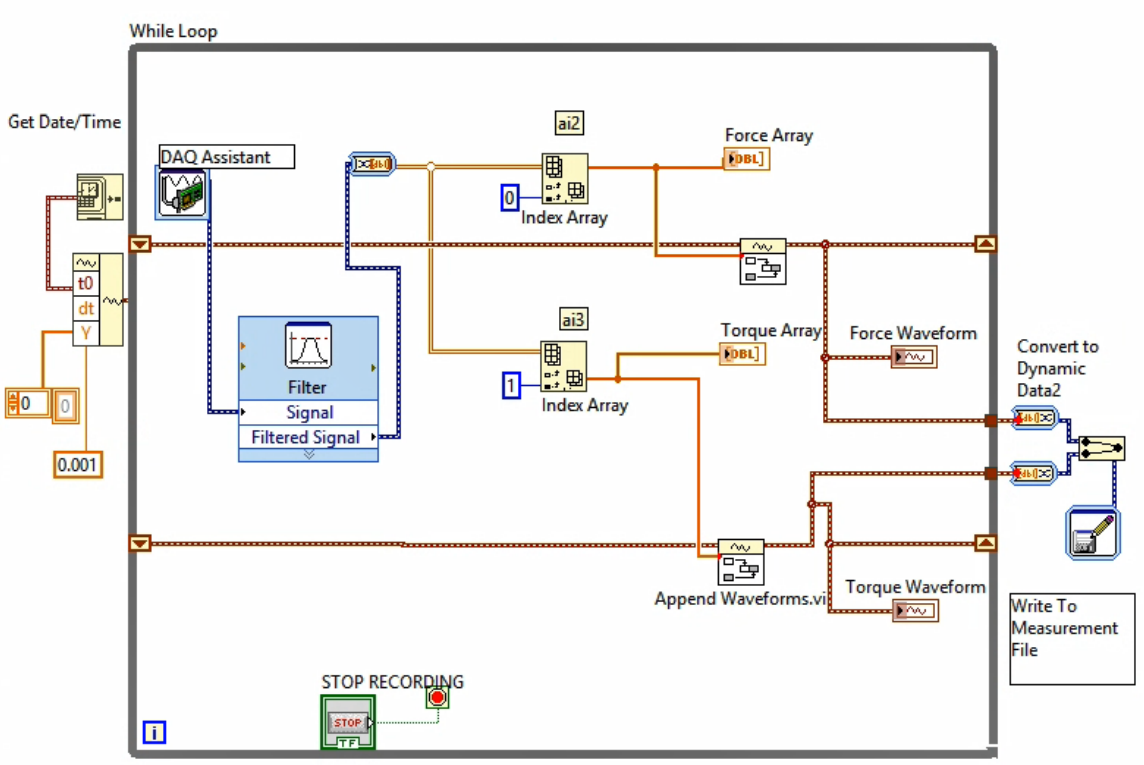

Figure 20 Block diagram for LabVIEW data acquisition

3.9 Cutting and surface preparation of cross section for microscopic examination

In order to evaluate the quality of the joint formed by the interference friction welding process, the cross section of the joint was needed to be studied. In order to obtain the cross section view for the study, the tube and the plate were cut through the center of the tube using Abrasive cutting machine as shown in Figure 21 that produces desired surface condition after the cut.

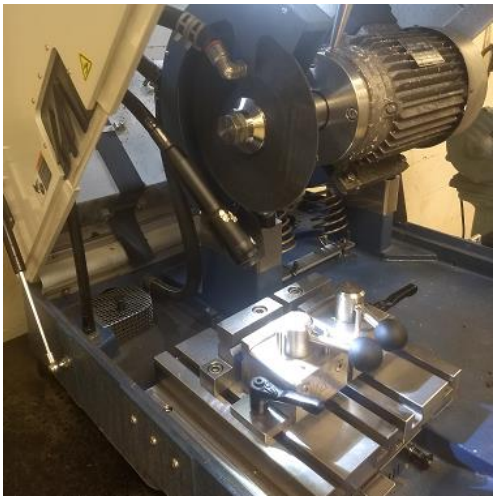

Figure 21 Abrasive cutting machine

Prior to that, the tube and the sheet metal plate were reduced in size to accommodate the assembly between the clamping blocks of the abrasive cutting machine. A coolant jet was applied through the nozzle to facilitate the cutting operation smoothly. It was important to obtain the cut with minimum cutting marks to evaluate the joint cross section accurately.

The clamping blocks of the abrasive cutting machine comprised of two pairs of mechanical levers for clamping the workpiece rigidly during the cutting operation as shown in Figure 22.

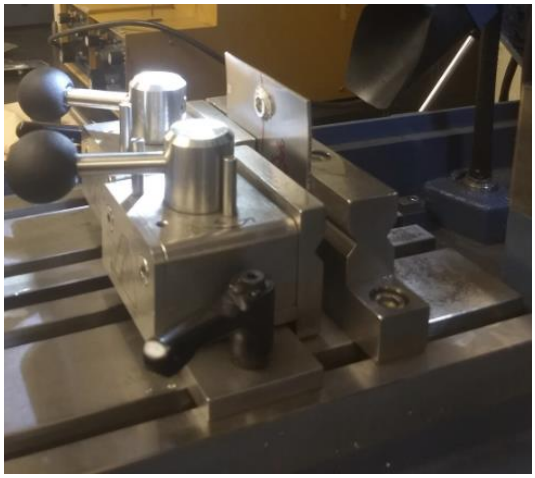

Figure 22 Clamping blocks

The larger pair of the levers were provided to position the specimen along the machine table with respect to the abrasive cutting wheel whereas the smaller pair of levers were provided for fine adjustment of the clamping blocks that ensured rigid clamping of the workpiece during the cutting operation. Despite using the abrasive machine, there were some cutting marks observed that needed to be removed to evaluate the joint. The cutting marks on the joint surface were removed by surface preparation technique. The surface was first cleaned with the CSM degreaser to remove the oil and grease followed by abrading and polishing the surface using 350 grit sand paper. Conditioner A was applied to the surface before evaluating the joint using the microscope. 1.3 MP Dino Lite microscope as shown in Figure 23 with 200X magnification capability and 1280×1024 pixels resolution was used to observe the joint.

Figure 23 1.3 MP Dino Lite microscope

The microscope comprised of adjusting screws to accommodate different dimensions of specimens by adjusting the height and angle of the lens. Dino Capture 2.0 software was needed to be installed to the computer in order to capture the microscopic images.

3.10 Mechanical testing setup description

The joints produced by the interference friction welding experiment were subjected to push (shear) test using United STM-100KN Testing System. The United Smart STM-100KN testing machine as shown in Figure 24 is a computer inclusive electro mechanical, Universal Testing Machine which is designed to operate in conjunction to variety of United test instruments and software, specifically for different types of metallic and non-metallic sample materials.

It can be utilized for both tension and compression (shear) testing. It is composed of two interconnected yet separate components:

1. The load frame where the actual testing of a specimen is performed.
2. The computer which controls the test process and handles all test data.

The load cell used was of 22400 lbs. capacity. The load cell is the force transducer that records the force and position data during the course of the shear testing process of the joints.

Figure 24 United STM-100 KN Testing system

DATUM is a windows based software program for conducting materials testing that was used for shear testing of interference friction welded specimens. DATUM requires a Pentium 4 or equivalent pc compatible computer with minimum 1 GB of RAM (2 GB when using Windows Vista or Windows 7) and Microsoft Windows XP professional or

Vista Business. DATUM requires MS access to store and retrieve test records and generate test reports. Several standard templates for different types of testing can be stored within the system. The template includes the basic structure of the testing procedure in a sequential manner starting from preloading to the final retraction of the load cell to its home position. The entire process is divided into preloading stage, loading stage and the unloading stage. There is a provision to generate prompts for the user after the end of each stage to enter comments. The control parameters like rate of loading, amount and rate of pre loading, total displacement of the load cell were required as an input from the user for the shear testing of the joints.

4 INTERFERENCE WELDING EXPERIMENT

4.1 Introduction

The aim of the experimental study was to check the feasibility of solid state diffusion bond formation between a rotating tube and a plate and study the axial and tangential forces (obtained from torque generated at the interface) for different set of parameters. The cross section microscopic analysis was done to check the formation of a diffusion bond between the mating surfaces. The strength of joint was also evaluated through a push test as discussed in the earlier chapter.

After setting up the data acquisition system components, balancing and calibration, the stationary plate was clamped to the fixture. Different set of experiments were performed to investigate the influence of process parameters on the axial force and tangential force/torque at the interface and correlate it to the heat generation at the interface due to friction and plastic deformation contributing to the quality of solid state joint being formed.

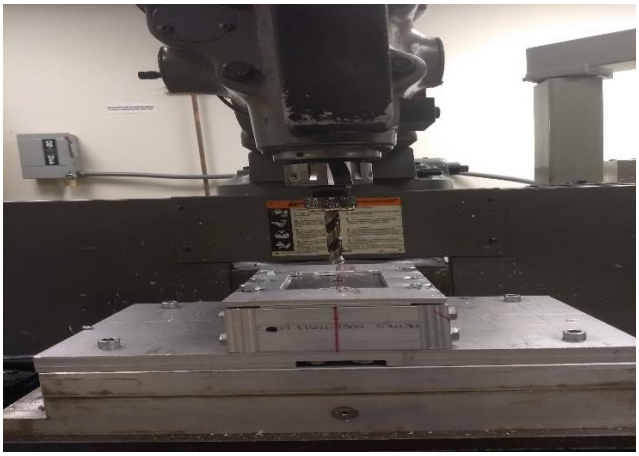

Figure 25 Hole drilling operation in the clamped stationary plate using a twist drill

Depending on the amount of interference required for the experimental trial, corresponding size of the drill bit was mounted on to the machine using a tool holder as indicated in Figure 25. A hole was drilled at the fixed location close to center of the plate which was maintained consistent for all the experimental trials. In order to achieve dimensional accuracy and uniform interference across the circumference of the joint, it was crucial to maintain the concentricity of the tube with respect to the drilled hole. In order to achieve that, the x and y coordinates of the machine table and the spindle are maintained the same throughout the experiment. After drilling the hole, the machine table was lowered along the z direction and the drill bit was removed. The tube specimen was inserted into a 0.5 inch tool holder and mounted on the machine spindle as shown in Figure 26 and Figure 27 respectively.

Figure 26 Tube holder assembly

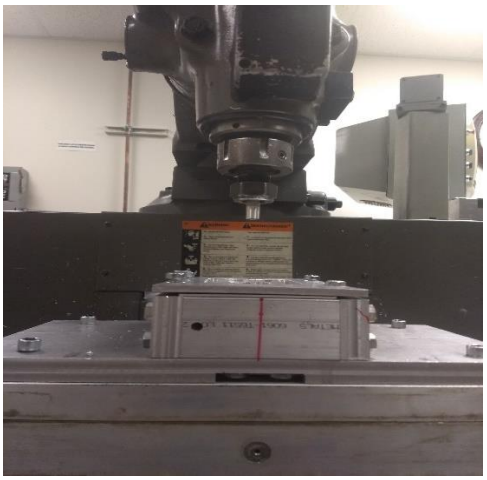

Figure 27 Interference Friction Welding setup

Since there was no change in the machine table x and y coordinates, the tube axis was in perfect alignment to the axis of the drilled hole. An automatic feed to the tube was provided by feeding in the G-code to the machine. The feed rate and spindle speed was maintained constant during the experiment. A tachometer was used to verify the spindle speed before running the experimental trial. The penetration depth of the tube was fixed by feeding the final z coordinate of the tube with respect to the surface of the specimen plate in the G-code fed to the CNC machine. After feeding the input parameters, the spindle was rotated at desired high rpm selected for a given experimental trial and fed into the specimen plate till the tube reached the final z-coordinate. As the rotating tube comes in contact with the stationary plate, the tube and the plate material at the interface experience plastic deformation which breaks the oxide layer of the aluminum specimens which allows the base metals to interact with each other that promotes solid state bond formation. The plastic deformation and the frictional sliding between the mating surfaces of the specimens contributes to the excessive heat generation at the interface which leads

to diffusion bond formation. Once the tube reached the final position defined by the G code z-coordinate, the tube rotation was stopped manually and the plate material experienced a relieve back which was observed during the experiments and reflected in the results of the experimental analysis. The material behavior of the rotating tube and stationary plate during the experimental trials and the effect on the thrust force and torque generated due to interference at the interface between the tube and the specimen plate during each of the experiment trials will be discussed in the subsequent section.

After the spindle was stopped after a successful trail, it was observed that the tube was joined to the stationary plate and hence it was necessary to remove the tool holder first from the machine spindle using a radial wrench along with the tube-plate assembly from the fixture by unfastening the bolts on the fixture. The tube plate assembly along with the tool holder was clamped on a bench vice and the tube was released from the tool holder for subsequent investigation of the joint.

4.2 Repeatability test for thrust force and torque

In order to ensure that the experimental setup provides a consistent and reliable data acquisition for the thrust force and torque at the interface, 3 dedicated experimental trials were performed keeping all the process parameters as constant. From the literature review, it was clear that all the friction welding applications operate at spindle speed range of 1000 rpm and above (typically between 1000 rpm to 3000 rpm). Hence the spindle speed was set to 2500 rpm for the repeatability study. The spindle speed was verified using a tachometer. The feed rate was set to be 8.46 mm/s (20 in./min) and the penetration depth of the tube was set to be 15 mm with reference to the top surface of the plate.

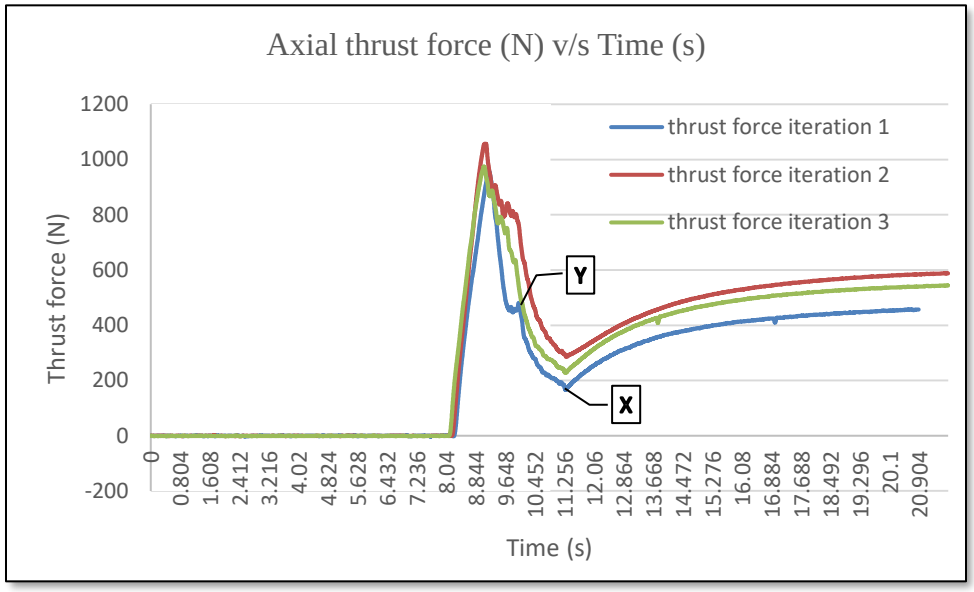

Figure 28 Thrust force repeatability check 2500 rpm feed rate 8.46 mm/s

The plate thickness for the trial was 2 mm and amount of radial interference selected for the repeatability experimental trials was 0.635 mm (0.05 in.). Accordingly, the drill bit was selected and a hole of diameter 11.43 mm (0.45 in.) was drilled as the tube

diameter for the experiments was 12.7 mm (0.5 in.). Figure 28 depicts the repeatability observed in the trend of the thrust force recorded at the interface. For all the 3 trials, as the tube comes in contact with the top surface of the plate and penetrates through the plate, the thrust force shoots up linearly till it reaches the peak value and then it decreases at a faster rate till it reaches the final penetration depth represented by point Y on the force trend in the Figure 28. The difference in the trends in the relieve back zone is due to the difference in the time taken by the user for the manual shutoff of the machine spindle as depicted by point X in the Figure 28, once it reaches the final z coordinate defined in the G-code fed to the CNC machine.

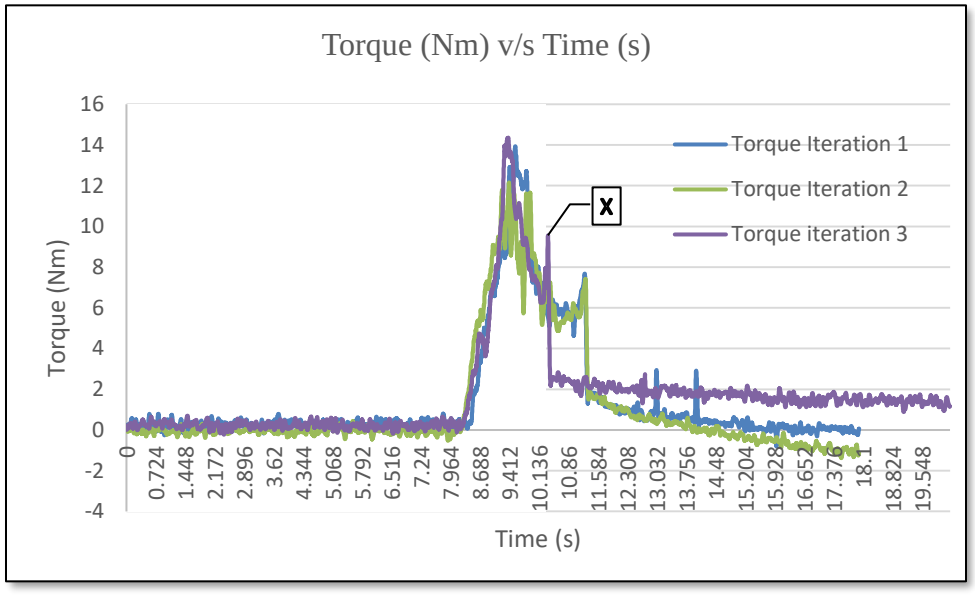

Figure 29 Torque Repeatability check 2500 rpm feed rate 8.46 mm/s

Figure 29 depicts the repeatability observed in the trends for the torque values recorded by the data acquisition setup. As the rotating tube penetrates into the drilled hole of the stationary plate, the plate material opposes the rotation of the tube as a result of

frictional sliding and hence a net torque is developed at the interface which is sensed by the strain gauges of the table mounted dynamometer.

The net torque values for all the 3 trials are observed to increase linearly initially and after it reaches the peak value there is a faster drop in the torque till it increases again because of the sudden stoppage of the rotation of the tube. The trend has been observed to be similar for all the 3 repeatability trials.

Point X for all the force and torque trends represents the turning off of the machine spindle rotation and point Y represents the stoppage of the axial feed of the tube.

4.3 Axial thrust force measurement results at different penetration depths

In order to study and understand the trend curves of thrust force to the interference friction welding process, the thrust forces were recorded at different penetration depths of the tube into the stationary plate with the drilled hole. The spindle speed, feed rate and amount of interference were maintained constant during all the iterations for this set of experiments.

It was observed that as the rotating tube comes in contact with the plate and continues to penetrate through the plate, the thrust force increases in a linear manner. Points A, B and C in Figure 30 depict the peak thrust force when the maximum penetration depth was defined to be 2 mm, 4 mm and 5 mm respectively. It was observed that the peak thrust force occurred at the maximum penetration depths and reduced after attaining the peak values for these 3 experimental trials.

Points D, E, F and G in Figure 30 depict the 9.4 mm, 12 mm, 15 mm and 20 mm penetration depths respectively. For these experimental trials, it was observed that the

thrust force attains the peak value before reaching the user defined penetration depth. This can be explained by the fact that as the rotating tube interacts with stationary plate, there is substantial amount of plastic deformation and frictional sliding which contributes to sufficient amount of heat generation that causes the material to get softer as it loses its strength with the increase in the temperature at the interface location.

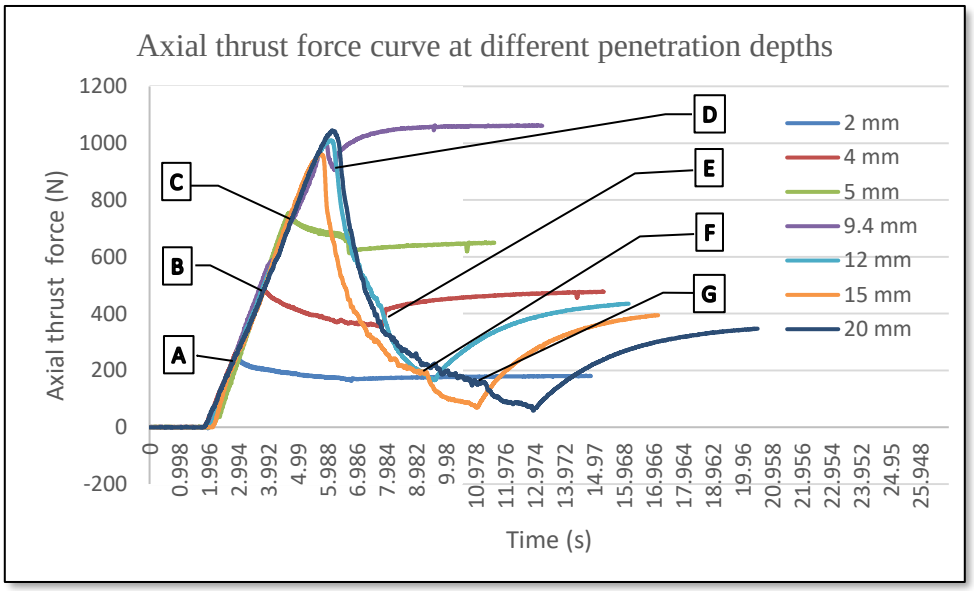

Figure 30 Thrust force measurement at different penetration depths

During the 7 iterations performed at different penetration depths of the tube from the plate surface, it was observed that as the rotating tube penetrates through the plate, the thrust force increases till it reaches a particular maximum value after which there is a steep drop in the axial thrust force. It was also observed that as the tube penetrates the through thickness of the plate, the thrust force drops at even steeper rate till the tube reaches the final z coordinate location fed into the machine which is evident for 12 mm, 15 mm and 20 mm penetration depths as shown in Figure 30. This behavior from the plots is the result

of the fact that as the tube penetrates through the complete thickness of the plate, the effective contact surface area at the interface increases and hence the frictional heat generation causes the material to get softer at much higher rate which causes the steep drop in the thrust force that has been recorded.

As soon as the rotation of the spindle is stopped, the material cools down suddenly due to larger surface area to volume ratio and experiences a relieve back which is observed by the increase in the thrust force. It was noted that the relieve back was prominent and greater for penetration depths of 9.4 mm and higher as compared to lower penetration depths of the tube where the tube does not penetrate through thickness of the plate.

4.4 General thrust force- torque behavior for interference friction welding process

The general trend in the recorded values of the thrust force and the torque generated at the interface as the rotating tube penetrates through the drilled hole in the stationary plate is depicted in Figure 31.The particular trend depicted above has been recorded at an interference level of 0.635 mm, spindle speed of 2500 rpm, feed rate of 8.46 mm/s and penetration depth of 15 mm from the top surface of the plate. However, the thrust force-torque trend has been observed to be consistent for all the experimental parameters whereas the peak values and slope of the linear region may differ.

It has been observed that as the rotating tube came in contact with the stationary plate and started penetrating the drilled hole, the axial thrust force value increased linearly at a faster rate as compared to the torque at the interface which is the result of resistance offered by the stationary walls of the drilled hole to the rotation of the tube in the rotational direction.

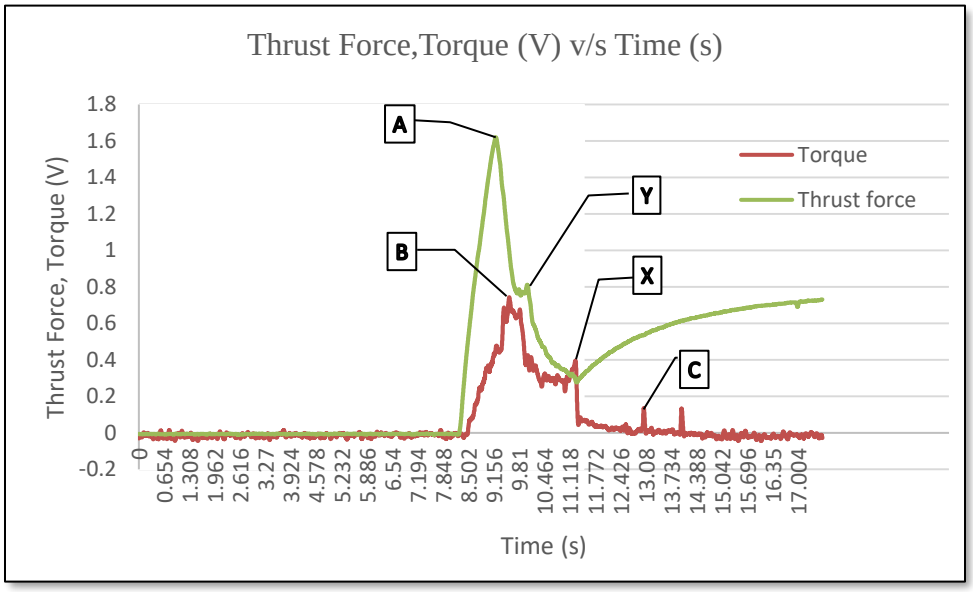

Figure 31 Thrust force-Torque characteristic trend for interference friction welding process

Furthermore as a result of heat generation, the resistance offered by the plate material to the axial feed motion of the tube reduced at a much faster rate after attaining the peak value depicted by point A. However, the torque generated at the interface continued to increase till it attained the peak value depicted by point B, as a result of increased coefficient of friction at the interface due to plastic deformation and steady feed of the tube.

Further, as the tube reached the final penetration depth as depicted by point Y defined by the user in the G-code fed to the CNC machine, a sharp drop in the torque and the thrust force was observed after a momentary increase in the both the parameters. As the tube was no longer penetrating in the axial direction, the heat generation at the

interference caused the tube and the plate material to get softer and the material was no longer able to offer resistance in the rotational direction.

Hence, the torque values were observed to decrease at a much faster rate after attaining the peak value along with drop in the axial thrust force values. As the machine spindle is turned off by the user and the tube suddenly stops rotating as depicted by point in X in the plot, there is a momentary rise in the torque followed by a sudden drop in the values. For some of the experimental trials it was observed that the torque values did not drop to the zero value even after the tube rotation was stopped. Though on releasing the tool holder from the machine spindle depicted by point C, it was observed that the torque values returned to the zero/initial value. On the other hand as explained in the previous section , at point X as the rotation of the tube is stopped, the heat generation stops and the material regains its strength and a relieve back in the axial thrust force values was observed.

The influence of different process parameters on the axial thrust force and the torque generated at the interface as a result of change in heat generation has been discussed in subsequent subsection.

4.5 Effect of different parameters on axial thrust force

The current subsection describes about the experimental observations about the influence of different parameters on the thrust force offered. The variation of the torque discussed in subsequent subsection and thrust force discussed in current subsection, under the effect of different parameters will be a good indicator of the tube plate interaction causing the heat generation at the interface that causes change in the material properties at the interface.

4.5.1 Effect of feed rate

For this set of experimental trials, the objective was to study the influence of the feed rate of the tube on the thrust force and torque at the interface for a constant spindle speed and amount of interference between the tube and the drilled hole in the stationary plate. This study was performed at feed rates 2.116 mm/s, 4.233 mm/s and 6.35 mm/s. The spindle speed and amount of interference were maintained constant at 1250 rpm and 0.635 mm respectively for all the 3 experimental trials.

From the Figure 32, it was observed that the slope of the linear zone of the thrust force plot got steeper with the increase in the feed rate of the tube. The magnitude of the peak thrust force was observed to increase with the increase in the feed rate. This can be attributed to the fact that with the increase in the feed rate of the tube through the plate, the interaction time between the rotating tube surface and the inner walls of the drilled hole in the stationary plate reduces and hence the amount of heat generation at the interface reduces. Since it was observed that the heat generation caused the material to get softer as a result of reduction in strength of the material, the material because of lower heat

generation, now offers higher reaction thrust force to the motion of the tube through the plate.

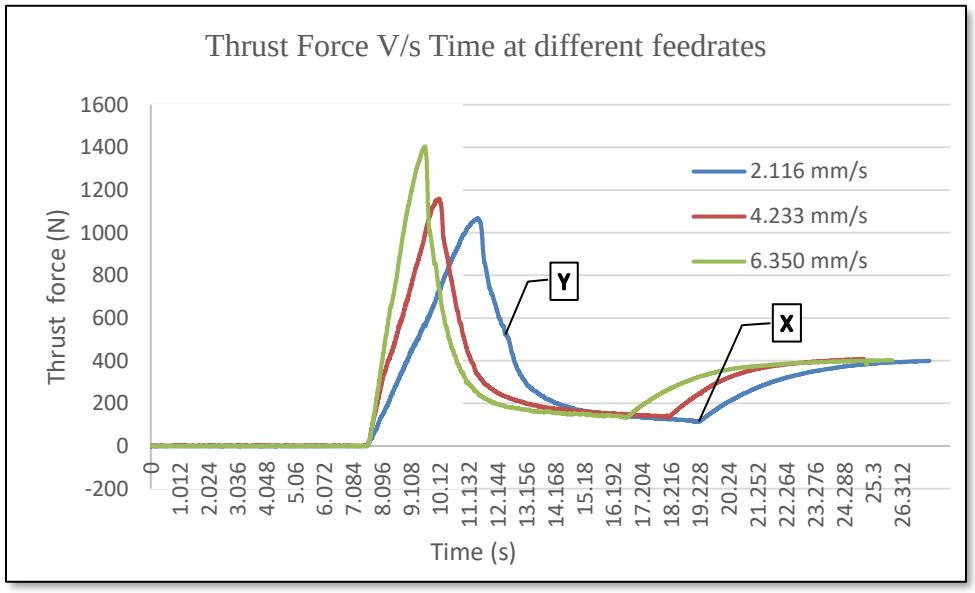

Figure 32 Thrust force measurement at different feed rates

4.5.2 Effect of spindle speed

From the literature review, it was realized that the spindle speed was the most influential parameter for the existing friction welding processes. In order to investigate the influence of spindle speed for interference friction welding process, experimental trials were performed at 5 different spindle speeds at a constant feed rate of 2.116 mm/s and amount of interference was 0.635 mm. The trends for the thrust force with the increase in penetration depth of the tube into the stationary plate were of similar nature as observed in the experimental trials for different feed rates. The general trend of the thrust force is observed to be consistent for all the spindle speeds where the thrust force increases linearly

till it reaches the peak value and drops non linearly after attaining the peak value. Excessive drop in thrust force after the tube reached the user defined penetration depth was observed at all the spindle speeds confirming the fact that as the feed of the tube was stopped, the excessive heat generation caused the tube and plate material at the interface to lose its strength, as a result of which the resistive torque at the interface drops substantially.

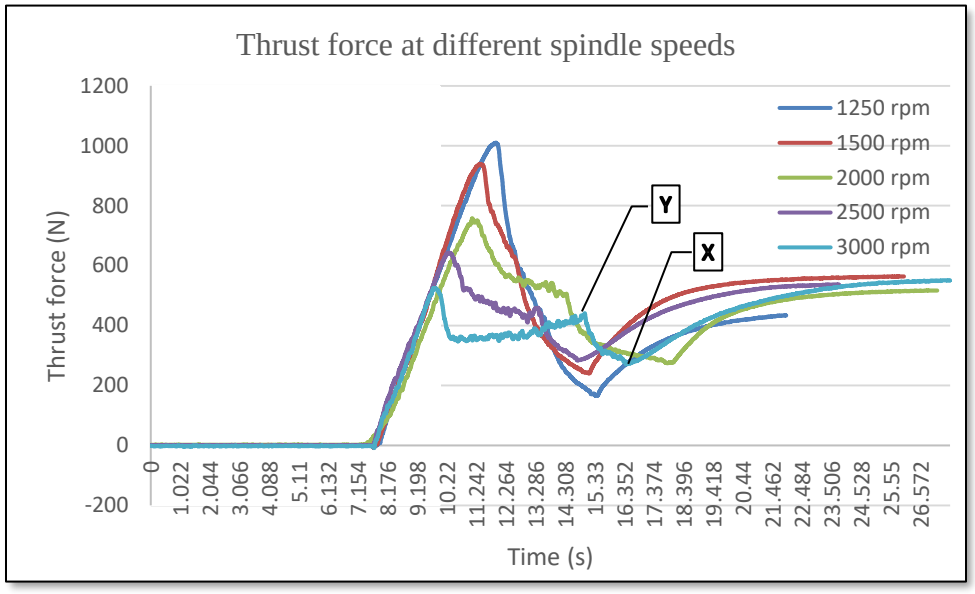

Figure 33 Thrust force measurement at different spindle speeds

With an increase in the spindle speed from 1250 rpm to 3000 rpm, the peak value of the thrust force reduced from 1010 N to 551 N as it can be observed from Figure 33. This substantial drop in the peak value of the thrust force can be attributed to the fact that with an increase in spindle speed, the rate of heat generation per unit length of the travel of the tube through plate increases which caused the material to soften at a much faster rate. As a result of higher heat generation rates at increased spindle speeds, the tube

experiences substantially lower amount of resistance in the axial direction as it penetrates through the plate thickness.

4.5.3 Effect of amount of interference

The effect of amount of interference on thrust force was studied at 3 difference interference levels. For a constant feed rate of 8.46 mm/s, spindle speed of 2500 rpm and penetration of 15 mm from the top surface of the stationary plate, the experimental trials were performed at 0.2032 mm, 0.3175 mm and 0.635 mm interference. Figure 34 shows the trend of the thrust force observed for different amount of interference between the rotating tube and the stationary plate.

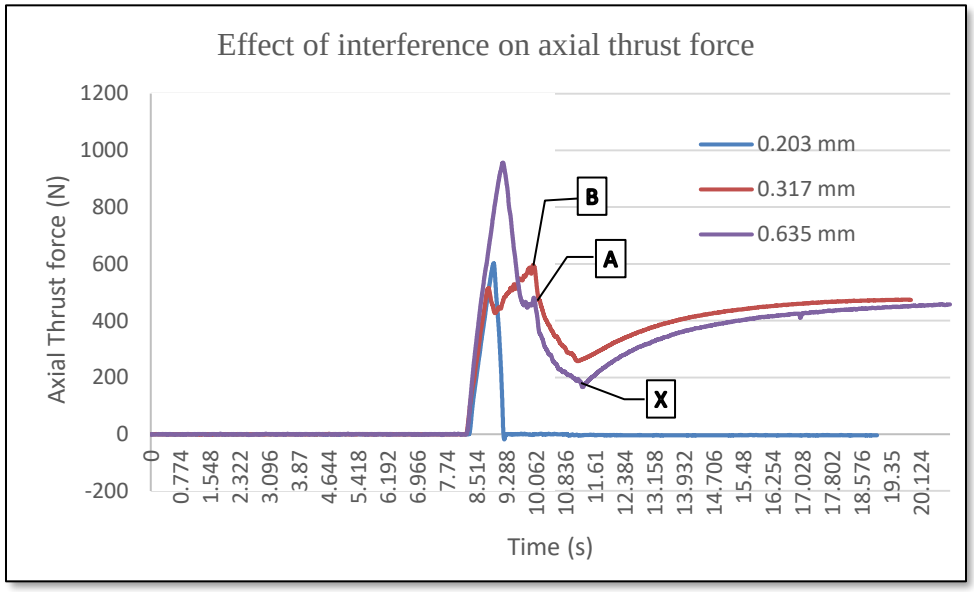

Figure 34 Thrust force at different interference levels

It can observed from Figure 34 that the amount of interference has a notable influence on the reactive thrust force offered by the stationary plate to the axial feed of the tube.

The thrust force increases linearly for 0.635 mm interference between the tube and the drilled hole as the plate material offers reactive force to tube feed in axial direction till the material at the interface becomes soft by the frictional interaction between the rotating tube and the walls of the drilled hole of the stationary plate. The thrust force drops at a much faster rate after the tube axial feed is stopped once it reaches the final penetration depth as depicted by point A in Figure 34.

As the tube rotation is stopped, the source of heat is cut off, the heat dissipates away rapidly as a result of which the material at the interfaces regains its strength and exhibits a relieve back effect. For the interference levels of 0.3175 mm, two peaks have been observed in the thrust force trends. In order to check the consistency of the trends, the same experiment was repeated twice and a repeatability in the trend was observed. The thrust force achieves the first peak before it crosses the entire thickness of the plate material, which can be estimated by the feed rate of the tube and the frequency of the signal recording. This observation can be understood from the fact that since at the interference level of 0.3175 mm, there is lesser material that interacts at the interface, the thrust force starts to drop before the tube crosses the entire thickness of the plate material.

Furthermore, as the unheated tube material continues to penetrate through the interface, the reactive thrust force again starts to increase till it achieves the final peak value depicted by point B in Figure 34. Further when the interference is reduced to 0.2 mm, it was observed that the rotating tube and the plate material subjected to the interference offer resistance till the heat generation at the interference causes the material to soften and displace from the weld location. This can be understood looking at the

sudden drop in the thrust force till it becomes zero, after the peak value was attained unlike observations for higher interference levels. Hence for 0.2 mm interference, it was observed that the interference between mating surfaces was not enough to create a friction joint for the given spindle speed, feed rate and the penetration depth of the tube.

4.6 Effect of different parameters on the torque

The current subsection describes about the experimental observations about the influence of different parameters on the torque generated at the weld interface as the result of the resistance offered by the stationary walls of the drilled hole to the rotation of the tube.

4.6.1 Effect of feed rate

It was also observed that as the feed rate increased from 2.116 mm/s to 6.35 mm/s, the torque generated at the interface by the interaction between the rotating tube and inner surface of the drilled hole also increased in magnitude. However, the change in magnitude of torque was not substantial in comparison to the change in thrust force. In addition, it can be observed from Fig. 35, that the torque increased at a faster rate as the feed rate increased from 2.116 mm/s to 6.35 mm/s. The trend of the plot can be seen shifted towards the left with the increase in feed rate. As the rotating tube penetrates through the plate thickness and slides against the stationary walls of the cylindrical hole, a torque is generated at the interface because of the resistance offered by the plate material in the tangential direction opposing the rotational motion of the tube. As a result of the frictional resistance to rotation of tube in tangential direction, there is substantial amount of heat generation that causes the temperature at the interface to rise and soften the material.

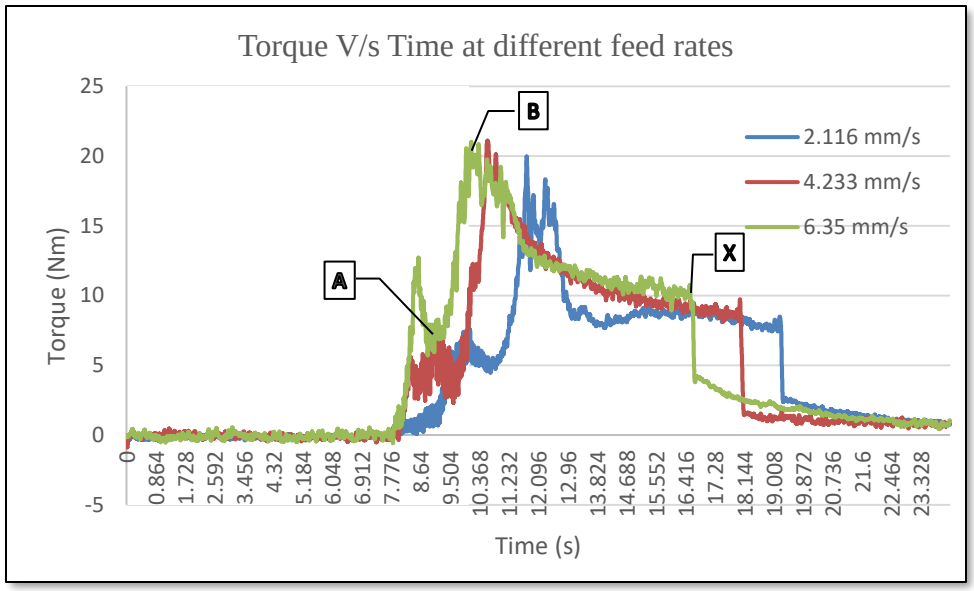

Figure 35 Trend of the torque values recorded at different feed rates

At higher feed rates, the tube experiences higher rotational resistance and hence higher torque, as the unheated tube material is fed into the heated plate material at a faster rate. However, eventually as the tube crosses the plate thickness the maximum cross section of the plate is exposed to the tube surface which results in higher heat generation causing a drop in the resisting torque which is observed as point A in Figure 35. Further as the tube continues to penetrate through the plate, the torque increases till it reaches the maximum penetration depth defined in the G-code. The point B in the Figure 35 depicts the peak torque value for feed rate of 6.35 mm/s. Once the axial feed of the tube is stopped, the torque continues to decrease as the material gets softer till the spindle is stopped manually by the operator. Same trend was observed for all the three trials at different feed rates.

4.6.2 Effect of spindle speed

It can be observed from Figure 36, that the trend of the torque generated at the interface at all the spindle speeds is similar to that observed for previous experimental trials. Though, the resistance offered by the plate opposing the rotation of the tube at the interface follows the similar trend as observed at lower rotational speed, for the same feed rate of the tube, the torque attains the peak value at a much faster rate and there is a steeper drop in the torque after the tube reaches the final penetration depth. This is due to the excessive heat generation at the higher spindle speeds. In addition, the magnitude of the peak value of the torque was also observed to drop with an increase in the spindle speeds as depicted by points A, B and C respectively in Figure 36.

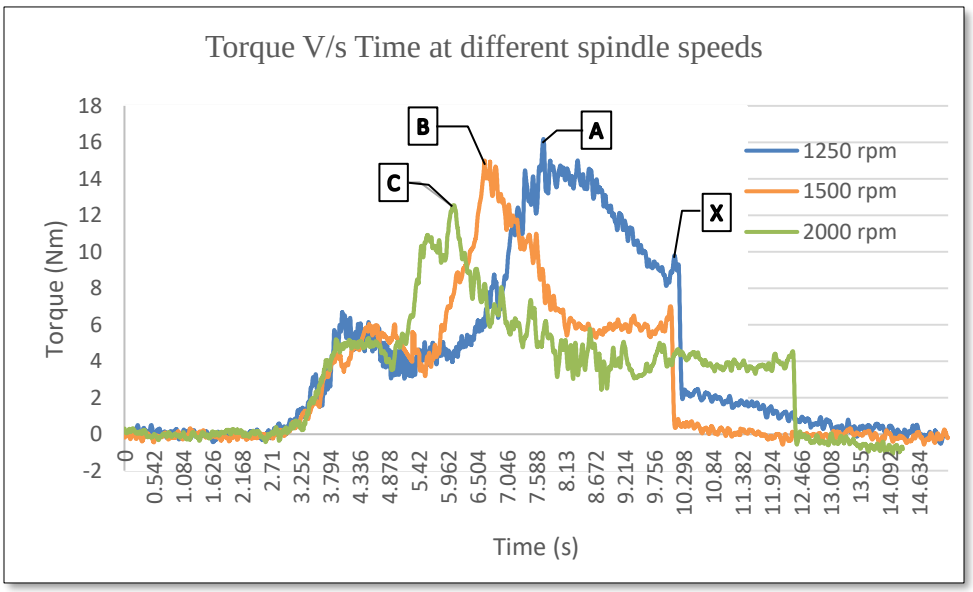

Figure 36 Trend of the torque values recorded at different spindle speeds

4.6.3 Effect of amount of interference

In order to study the influence of amount of interference, the torque generated at the interface was studied at three different amount of interference. It was observed that for 0.2032 mm interference, the torque increased linearly just as other two iterations at higher interference levels, however the torque rapidly dropped to zero after attaining the peak value as it can be observed from Figure 37.

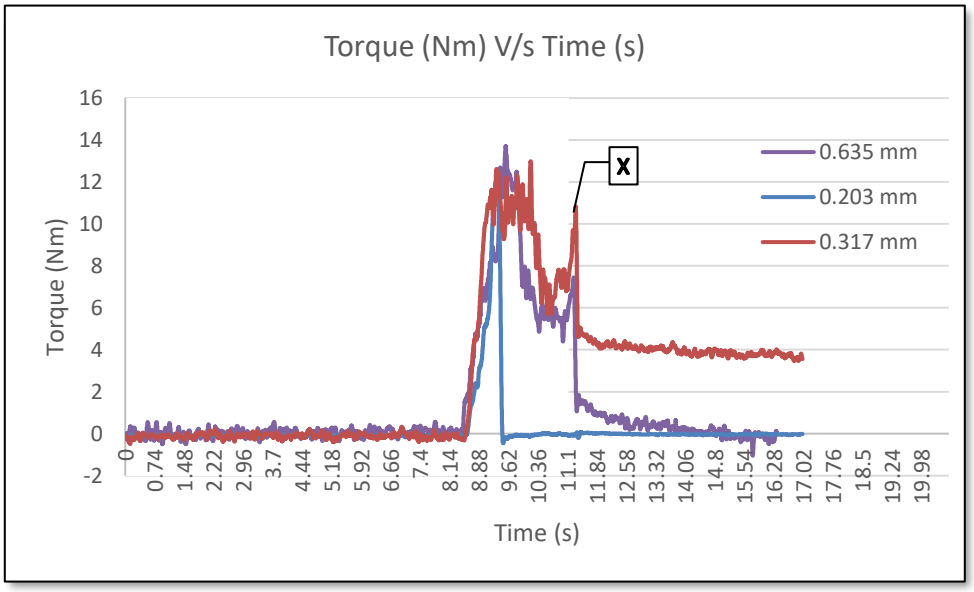

Figure 37 Trend of torque values at different amount of interference

The reason for this behavior can be attributed to the fact that as the torque increased, the heat generation at the interface increased. Due to lower amount of interference at the peak torque, the material became softer and was displaced from the joint location. Hence, there was no interference left between the rotating tube and the walls of the hole in the stationary plate. From this observation it was clear that the interference at the joint location should be sufficient enough so that the material does not get displaced

due to the excessive heat generation due to frictional sliding. Furthermore, it was observed that the peak value of the torque at the interface for 0.635 mm and 0.3175 mm interference levels was not much affected by the amount of interference. Hence in order to ensure consistent formation of solid state sound weld joint, it is critical that there is continuous contact between the rotating tube and the walls of the stationary plate throughout the interference friction welding experiment. The time period for the process is solely dependent on the feed rate of the tube and the penetration depth defined by the user in the G-code fed to the CNC machine.

4.7 Observations from interference friction welding process trials with microscopic analysis

As discussed in the section 3.9, in order to evaluate the joint quality and the influence of different process parameters, the joint was subjected to a microscopic examination discussed in the subsection below and shear testing of the welded joints which has been discussed in the subsequent subsection.

It was observed that for certain process parameters like at lower spindle speeds around 1000 rpm, constant feed rate 2.11 mm/s, lower amount of interference less than 0.2 mm and thickness of the plate specimen less than 1.5 mm, the tube plate interference did not generate the required amount of interaction to cause sufficient heat generation that would lead to softening of the material. As a result in some cases the tube did not bond at all with the walls of the drilled hole and was separated from the plate material as the tool holder was released from the machine spindle. Hence, it was clear that the diffusion bond formation was not successful for those set of parameters.

From the observations of the parametric study of trends of thrust force and torque, it was clear that the rate of heat generation was higher for higher spindle speeds and lower feed rates. As a result, it was observed that the material at the interface got softer till the final penetration depth of the tube was reached. In addition, it was known from the literature review that the coefficient of friction at the interface increases with increase in the temperature. Hence, in order to facilitate the formation of diffusion joint subsequent trials were performed at higher spindle speeds and at a low feed rate.

It was observed that on marginal increase of the spindle speed to 1250 rpm keeping the feed rate same, increase in the amount of interference to 0.635 mm and increase of plate thickness to 2 mm , the tube did not get separated from the plate even after the tool holder was released from the machine spindle. Hence it was necessary to investigate the root cause of joining of the tube to the stationary plate, whether it was as a result of mechanical locking or there was a diffusion bond that was being formed. It was expected that if the joint between the tube and plate was a result of mechanical locking, then on cutting the cross section of the joint using abrasive cutting machine as discussed in section 3.9, the tube specimen would separate from the plate. However, for the joints created by the above mentioned parameters, it was observed that the tube specimen was bonded to the plate only at some local points and a crack was observed at the interface as shown in Figure 38.

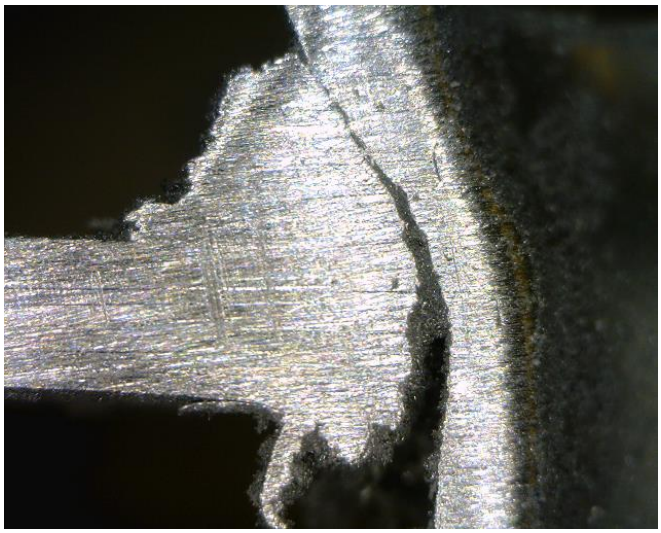

Figure 38 Microscopic image of the joint formed at spindle speed 1250 rpm, feed rate 2.116 mm/s, interference 0.635 mm, plate thickness 2 mm

Further, the spindle speed was increased to 1500 rpm, keeping the feed rate, amount of interference and plate thickness the same. It was observed that the given set of parameters fetched better results, however a fine crack was visible in the microscope at one of the interface edges as shown in Figure 39.

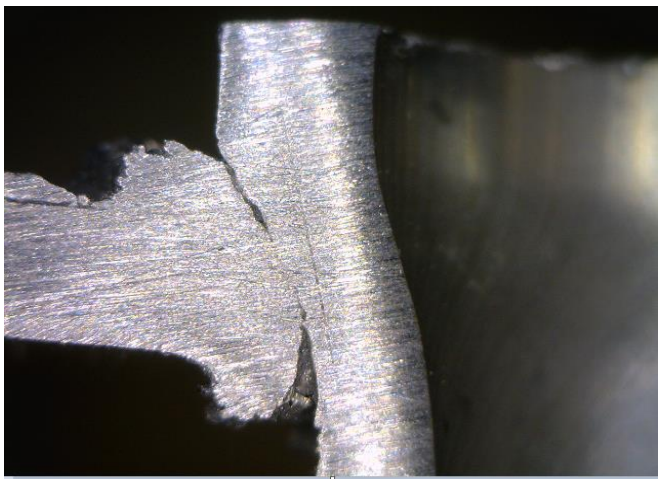

Figure 39 Microscopic image of the joint formed at spindle speed 1500 rpm, feed rate 2.116 mm/s, interference 0.635 mm, plate thickness 2 mm

Hence, it was clear that in order to obtain a uniform diffusion joint by generating required amount of heat, the rate of material contact between the surfaces was needed to be increased.

In order to increase the heat generation rate at the interface, the spindle speed was increased to 2000 rpm, keeping the feed rate and amount of interference the same. The Figure 40 (a), (b) represents the joint image captured by the microscope. For this set of parameters, a partial crack was observed in some of the specimens and hence for a uniform bonding of the specimens, the parameters were needed to be optimized further.

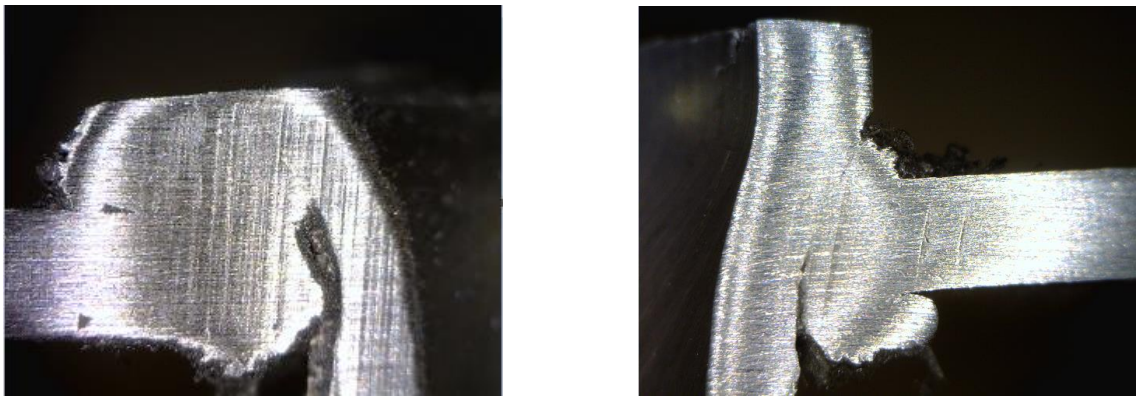

(a) **(b)**

Figure 40 (a), (b) Microscopic image of the joint formed at spindle speed 2000 rpm, feed rate 2.116 mm/s, interference 0.635 mm, plate thickness 2 mm

In order to obtain the sound uniform joint throughout the circumference, the spindle speed was further increased to 2500 rpm keeping the feed rate and amount of interference constant at 2.116 mm/s and 0.635 mm respectively. However, it was observed that the increased heat generation rate as a result of increase in spindle speed caused the material to get softer and lose its strength at much faster rate.

The softened material was observed to get displaced from the weld interface as depicted in Figure 41 (a), (b), till the tube reached the user defined penetration depth which was maintained constant for all the spindle speeds. In order to match up the rate of heat generation at the interface at high spindle speeds like 2500 rpm, it was necessary to reduce the time taken by the tube to reach the final penetration depth. Hence for the subsequent experimental trials, the feed rate of the tube was increased to 6.35 mm/s. Despite the increase in feed rate, the softened plastically deformed material was observed to partly dislocate from the weld joint interface, and a void was created at the joint as depicted in Figure 41 (a), (b).

(a) (b)

Figure 41 Microscopic image of joint formed at spindle speed 2500 rpm, feed rate (a) 2.116 mm/s (b) 6.35 mm/s, interference 0.635 mm

In order to prevent the softened material to get displaced from the joint location, it was necessary to further increase the feed rate of the tube to limit the total heat generation at the interface during the entire process of tube insertion. Hence maintaining the spindle speed at 2500 rpm and all the other parameters the same as previous iteration, the feed rate of the tube was increased to 8.46 mm/s. On performing the microscopic analysis, a sound

joint without any cracks was observed at the joint interface which has been depicted in Figure 42 (a-i). In order to establish consistency for the process, several repeatability trials were performed for same set of parameters. For all the repeatability trials, the process exhibited a consistency in the results which was verified by the microscopic analysis and shear test results.

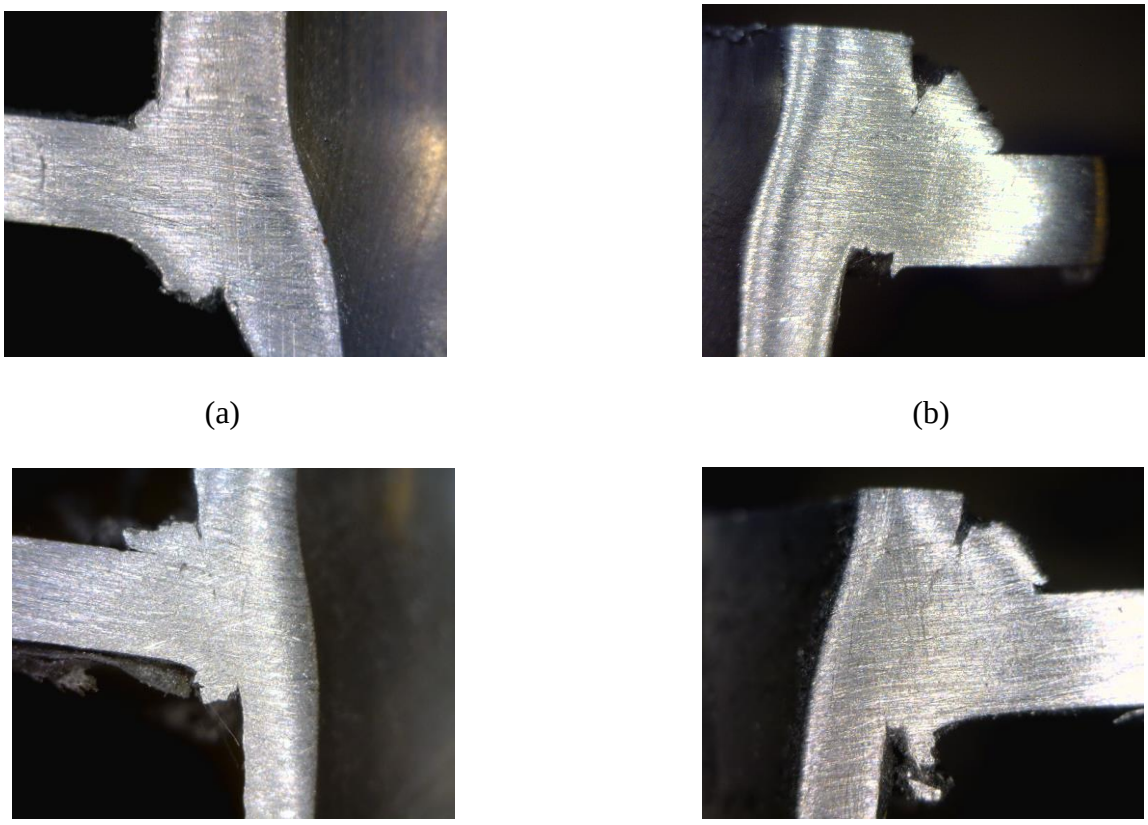

(a) (b)

(c) (d)

Figure 42 (a-i) Microscopic images of the joint formed at spindle speed 2500 rpm, feed rate 8.46 mm/s, interference 0.635 mm, plate thickness 2 mm depicting consistency of results

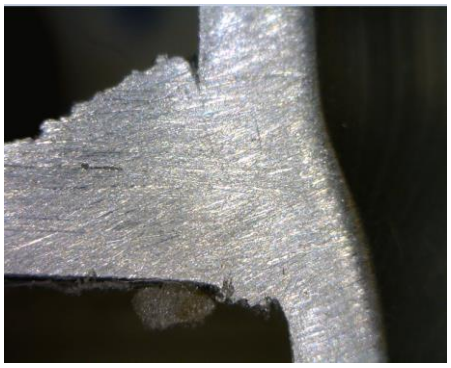

(e)

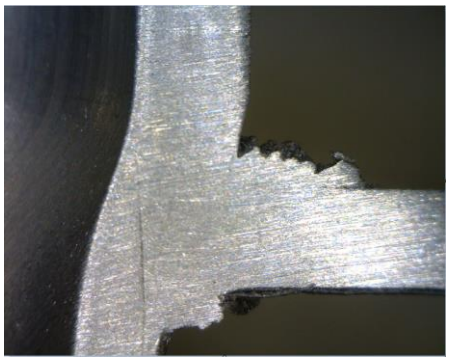

(f)

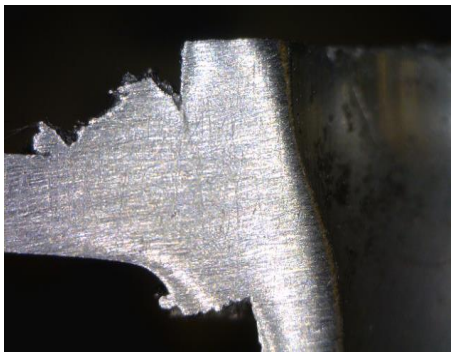

(g)

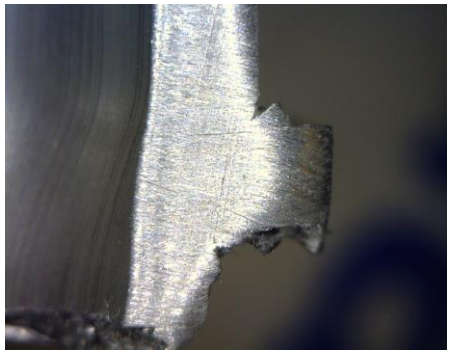

(h)

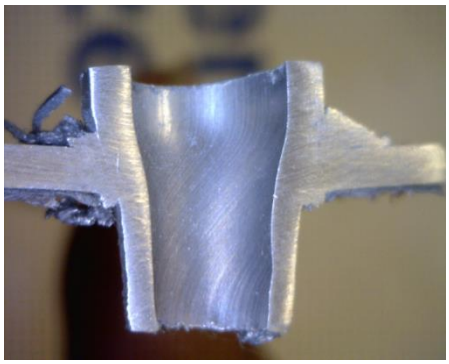

(i)

Figure 42: (a-i) Microscopic images of the joint formed at spindle speed 2500 rpm, feed rate 8.46 mm/s, interference 0.635 mm, plate thickness 2 mm depicting consistency of results (Continued)

4.8 Shear testing of the interference friction welded Joints

The joints created by interference friction welding process were subjected to shear test using the setup described in section 3.10. The tube plate assembly was mounted on a rectangular block with a hole as shown in Figure 43 (a), (b), to accommodate the tubular projection of the assembly and ensure that the entire load applied by the displacement of the load cell is applied at the tube-plate joint formed at the interface. The compressive force applied by the displacement of the load cell tends to apply a shear force at the joint that generates the shear stress sufficient enough to shear off the joint.

(a)

Figure 43 (a) Shear test setup (b) C-block with a hole with welded specimen

(b)

Figure 43 (a) Shear test setup (b) C-block with a hole with welded specimen (continued)

As discussed in section 3.10, the control parameters for the test are fed into the DATUM software using an inbuilt template that can be edited by the user in order to make changes to the testing parameters. Shear tests for interference friction welded joints at different process parameters were performed. Table 4 below includes the shear test results for joints formed at spindle speed of 1250 rpm. Looking at the results from the Table 5, it can be observed that the maximum shear force sustained by the joint or the shear strength of the joint is consistently low depicting the fact that the sound diffusion bond at 1250 rpm could not be formed.

	Parameters	Shear force (N)	Shear stress (MPa)
Spindle speed	1250 rpm		
Feed rate	2.116 mm/s		
Amount of interference	0.635 mm		
Tube penetration	12 mm	171.073	2.143
Spindle speed	1250 rpm		
Feed rate	2.116 mm/s		
Amount of interference	0.635 mm		
Tube penetration	12 mm	165.356	2.071
Spindle speed	1250 rpm		
Feed rate	2.116 mm/s		
Amount of interference	0.635 mm		
Tube penetration	12 mm	169.821	2.127
Spindle speed	1250 rpm		
Feed rate	2.116 mm/s		
Amount of interference	0.635 mm		
Tube penetration	20 mm	481.347	6.030
Spindle speed	1500 rpm		
Feed rate	2.116 mm/s		
Amount of interference	0.635 mm		
Tube penetration	12 mm	372.937	4.672

Table 5 Shear test results for spindle speed of 1250 rpm and 1500 rpm

Moreover, on increasing the penetration depth of the tube, the shear strength of the joint increased significantly as it can be observed from the readings in the Table 6. The reasoning for this observation is that on increasing the penetration depth keeping the feed rate constant, the total heat generation at the interfering faces increases due to longer interaction between the mating surfaces which leads to formation of diffusion joint at intermittent locations. Similarly, the shear strength of the joint for same feed rate, interference and tube penetration depth has been observed to increase with increase in the

rotational speed of the tube as the heat generation rate increases for the same travel distance of the tube.

	Parameters	Shear force (N)	Shear stress (MPa)
Spindle speed	2000 rpm		
Feed rate	2.116 mm/s		
Amount of interference	0.635 mm		
Tube penetration	20 mm	187.355	2.347
Spindle speed	2000 rpm		
Feed rate	6.35 mm/s		
Amount of interference	0.635 mm		
Tube penetration	12 mm	1751.944	21.948
Spindle speed	2500 rpm		
Feed rate	2.116 mm/s		
Amount of interference	0.635 mm		
Tube penetration	15 mm	1121.341	14.048
Spindle speed	2500 rpm		
Feed rate	6.35 mm/s		
Amount of interference	0.635 mm		
Tube penetration	15 mm	1647.250	20.637

Table 6 Shear test results for spindle speed of 2000 rpm and 2500 rpm

Based on the previous observations of the experimental trials and microscopic examination, the rotational speed of the tube was increased to 2000 rpm to obtain higher heat generation rates and the feed rate was increased to 6.35 mm/s to prevent the displacement of the softened material at the interface. The peak shear force sustained by the joint was increased substantially for the given increased spindle speed of 2000 rpm as compared to 1500 rpm.

In order to further investigate the effect of higher tube rotational speeds, the spindle speed was increased to 2500 rpm. It was observed that with the high spindle speed

of 2500 rpm and low axial feed rate of 2.116 mm/s, the heat generation caused the softened material to displace from the desired weld area and was also reflected in reduced shear load bearing capacity/reduced shear strength of the joint. Further on increasing the feed rate of the tube to 8.466 mm/s, the increased heat generation rate was compensated by the reduced time taken by the tube to reach the final penetration depth, thereby limiting the overall total heat generation at the interface.

	Parameters	Shear force (N)	Shear stress (MPa)
Spindle speed	2500 rpm		
Feed rate	8.466 mm/s		
Amount of interference	0.635 mm		
Tube penetration	15 mm	4444.361	55.680
Spindle speed	2500 rpm		
Feed rate	8.466 mm/s		
Amount of interference	0.635 mm		
Tube penetration	15 mm	4466.718	55.960
Spindle speed	2500 rpm		
Feed rate	8.466 mm/s		
Amount of interference	0.635 mm		
Tube penetration	15 mm	5011.578	62.786

Table 7 Repeatability check of shear test results for spindle speed 2500 rpm and feed rate of 8.466 mm/s

Hence, the maximum shear strength of the joint was observed at 2500 rpm, 8.466 mm/s feed rate of the tube for the given penetration depth of 15 mm from the top surface of the stationary plate. In order to check the consistency of the results at the given parameters, the experiment was repeated thrice and the results for all the three repeatability trials are shown in the Table 7 above.

Figure 44 below, shows the repeatability test results for the interference friction welded joints plotted from the Force and time data exported from the DATUM software.

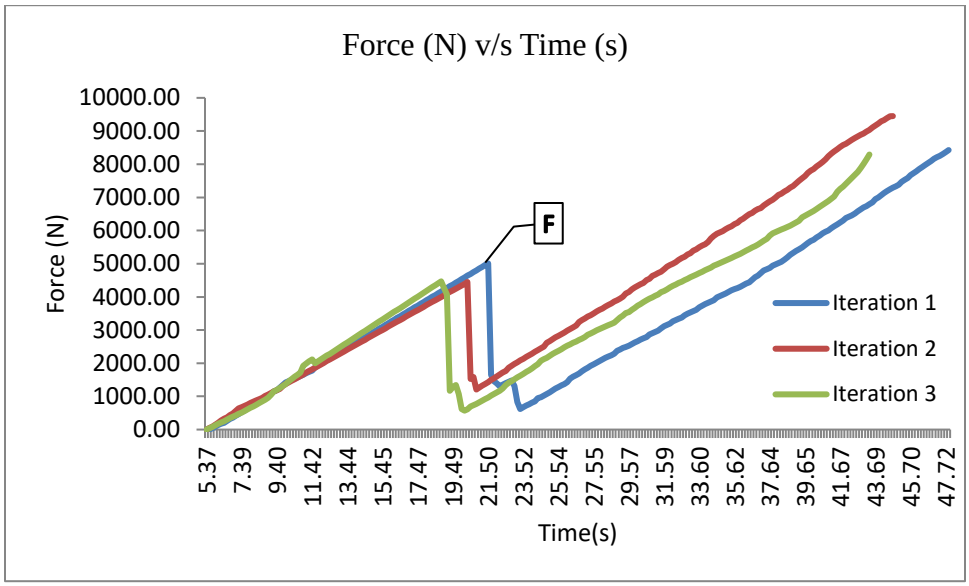

Figure 44 Force V/s Time trends for shear test results for joints formed at spindle speed 2500 rpm, feed rate 8.466 mm/s, 15 mm penetration from the top surface and 0.635 mm interference

It can be observed from trends that the shear force taken up by the joint increases till point F where the diffusion bond breaks and there is a steep drop in the load sustained by the joint. Further the joint did not collapse and the shear force taken up by the tube plate assembly increased because of the mechanical interlocking due to excessive surface roughness (seizure phenomenon) and plastic deformation of the tube plate interface. However after point F, the tube was observed to displace through the weld location with a consistent increase in the shear force till the projection of the tube from the bottom surface of plate became zero or the maximum displacement of the load cell was attained (whichever occurred first). The reason for the increase in the shear force could be

attributed to the fact the diameter of the tube was observed to increase under the compressive force effect at the end of the tube and the hole was filled up by the plastically deformed material due to heat generation. Hence, the additional net effect of this process was that an added interference was obtained between the tube and the plate material that prevented the tube to get separated from the plate material even after the diffusion weld joint collapsed. Figure 45 demonstrates the behavior described above.

(a) (b)

Figure 45 Joint location (a) top surface (b) bottom surface, post shear test

4.9 Shrink fitting of the tube plate assembly and comparison to interference friction welded joints

Shrink fits are interference fits that are created by heating one of the members whereas the other member remains cool. The specimens can then assembled with little or no force. As the heated material cools down, it shrinks back to its original state and an interference is achieved between the mating surfaces. Shrink fits can offer same dimensional interference as in case of force fits that are created by the application of external force. The temperature increase required to expand the specimen being heated depending on the amount of interference desired can be computed by the simple equation of coefficient of thermal expansion,

$$\delta = \alpha L (\Delta t) \quad [18] \tag{5}$$

where, δ = change in diameter required for cylindrical parts (mm)

α = coefficient of thermal expansion (in/in ·ºF or mm/mm ·ºC)

L= diameter for cylindrical parts (mm)

Δt = temperature difference (ºF or ºC)

For the given geometrical dimensions of the specimens in this study, the amount of interference was selected to be 0.04572 mm (0.0018 in.) from the standard tolerances for shrink and force fits given in [18].

In order to achieve the required amount of interference for this study, a hole of diameter 12.34 mm (0.4858 in.) was drilled using a 31/64 in. drill bit. The tube was turned down from 12.70 mm (0.5 in.) to 12.38 mm (0.4874 in.).

A Vernier caliper of 0.02 mm least count was used to measure the dimensions as shown in Figure 46. Hence, the overall required interference was achieved to be 0.04 mm.

(a)

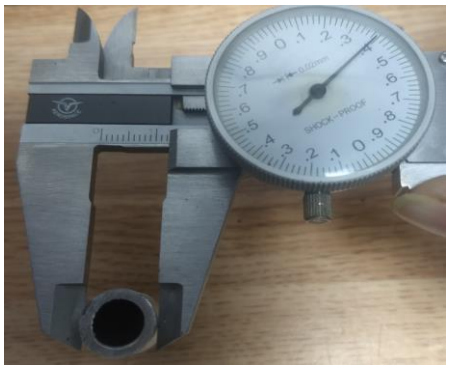

(b)

Figure 46 (a) I/D of hole, (b) O/D of tube measured using Vernier caliper with least count of 0.02 mm

In order to achieve a shrink fit joint for the given actual amount of interference, the temperature required to expand the drilled hole to the required amount was computed using the above equation for coefficient of thermal expansion. For Al 6061 material with coefficient of thermal expansion of 23.4×10^{-6} mm/mm·°C , mean hole diameter of 12.3 mm, and the minimum required deformation of 0.04572 mm , the minimum temperature

difference required was computed to be 158.81 ºC. In order to achieve the temperature difference, the plate with the required size of the drilled hole was heated in a residential induction oven. An infrared temperature gun was used to measure the surface temperature of the plate as shown in Figure 47.

Figure 47 Non-contact type of temperature measurement using IR gun

The plate was heated till the entire plate surface was at least at a temperature of 253.2 °C in order to ensure smooth insertion of the tube into the hole later on. Once the steady state temperature of the plate was attained where the temperature remained constant, it was removed from the oven using mechanical grippers and the tube was inserted into the hole manually. The plate was allowed to cool with the tube held concentric to the hole. As the plate cooled down to the room temperature, the size of the hole reduced than the outside diameter of the tube. As a result a shrink fit was created between the hole and the tube.

In order to compare with the interference friction welded joints, the shrink fit joints were subjected to a shear test. The maximum shear force sustained by the shrink fit joint was 865.795 N (194.397 lbs.). Hence, for the given joint, the shear strength of the shrink fit joint was computed to be 10.890 MPa. Figure 48 shows the shear testing of the shrink fit joint.

Figure 48 Shear test of Shrink fit assembly

5 ANALYTICAL MODEL

5.1 Introduction

In order to validate the experimental results, a simple analytical model was proposed based on the contact area and pressure considering the temperature dependent material properties which has been discussed in the latter part of this chapter. During the interference friction welding process, there is sufficient amount of heat generation that causes a change in the properties of the material. In order to form sound welds, there are two most important parameters that must be controlled, heat input and the material flow. The coefficient of friction does have an influence on frictional heat generation, whereas the interface condition has a major effect on material flow characteristics.

As the tube-plate surfaces interact, the plate and the tube material undergo a plastic deformation that contributes to the heat generation in addition to the frictional heating due to the rotation of the tube. The heat generation at the interface due to frictional sliding between the rotating tube surface and inner walls of the drilled hole is the product of the frictional force and the tangential velocity of the tube with respect to the stationary plate surface. Whereas heat generation per unit area/heat flux due to plastic deformation at the tube plate interface will be the product of the shear stress of the material and the tangential velocity of the tube.

The fundamental equations for heat generation at the interface used by P. Biswas and N.R.Mandal [19] for Friction Stir Welding are also applicable for the current study. Though a separate conical tool is used for Friction Stir Welding, the heat transfer analysis

for the cylindrical section of the tool can be compared with the cylindrical tube in the current study.

The frictional heat generation on an infinitesimally small element area ΔA at the interface due to friction between the tube rotating at high rotational speed as compared to axial feed rate can be expressed as,

$$dQ_{frictional} = (1 - \delta)\omega r \mu p dA \quad (6)$$

The heat generation due to plastic shear deformation causing the tube and plate material to stick is given by,

$$dQ_{plastic\ deformation} = \delta \omega r \tau_y dA \quad (7)$$

For equation (6) and (7), δ is the extent of slip, ω is the angular speed of the rotating tube, r is the mean radius of the interface, μ is the coefficient of friction, p is the contact pressure, τ_y is the shear yield stress of the tube and plate material.

Hence, the total heat generation due to combined friction and plastic deformation can be expressed as,

$$dQ = dQ_{plastic\ deformation} + dQ_{frictional} \quad (8)$$

$$dQ = \omega r dA[(1 - \delta)\mu p + \delta \tau_y] \quad (9)$$

The extent of slip in above equation can be compared to the slip calculated for Friction Plug Welding process as expressed in eq.(3) and eq.(4) in the literature review section. The empirical expressions for computing the extent of slip for Friction Plug Welding process were developed by Amitava et. al. [20] following similar expressions used in modeling of Friction Stir Welding process [21]. For Friction Stir Welding process the extent of slip was estimated from the functional relationship determined from the reported

experimental data of tool-workpiece interfacial slip in a flat wedge rolling process [22]. In the flat wedge rolling process, global slip has been defined as the difference in the distance translated by the forming tool and the linear distance rotated by the cylindrical workpiece during the specified forming period. Hence the extent of slip for interference friction welding process alike other friction welding processes can be compared with the flat wedge rolling process and the experimentally reported data can be used.

As previously discussed in the literature review, one important aspect while considering the frictional heat generation is the coefficient of friction at the interface. Several researchers have presented their empirical and analytical expressions for computing coefficient of friction at different temperatures and contact pressures, as direct measurement of the coefficient of friction is not feasible. A wide range of coefficient of friction has been presented from different research studies. The subsequent subsection of this chapter describes about the different models presented for considering the coefficient of friction.

5.2 Review of friction modeling

The existence, nature and severity of friction between variety of metals (similar or dissimilar) have been analyzed for different sticking and slipping conditions at various temperatures and contact pressures. Despite the prevailing discrepancy between the experimental value and theoretical value of coefficient of friction, in thermal modeling of Friction Stir Welding process the coefficient of friction was assumed to be 0.4-0.5 for the purpose of calculations at different temperatures and contact pressures. [23-27]. Schmidt and Huttel [28] in their study reported that coefficient of friction is assumed in many cases

instead of actual measurement. Thompson and Chen [29] with their theoretical approach presented that the coefficient of friction cannot be greater than 0.577 during friction welding whereas around the same time, Duffin and Bahrani [30] experimentally found the friction coefficient to exceed 0.57 during friction welding. They proposed the coefficient of friction values to be 1.5, 1.9, 2.1 and 2.7 for friction welding of mild steel material. Similar results were reported by Reid and Schey [31] for friction welding of pure copper. Chao et. al. [32] and Miller et. al. [17] in their FEM study of Friction Stir Welding process used an inverse method for friction to match experimental and modeling results for temperature. They got the results validated for coefficient of friction of 2.

5.3 Calculation of analytical axial thrust force and torque for interference friction welding process and comparison to the experimental results

For this study, the fundamental Coulomb friction model has been used. The model used by Miller et. al. [17] for conical shaped tip tool for Friction Stir Welding process can be applied for the cylindrical tube for the current study of interference friction welding process. The model is based on the contact pressure and contact area between the tube and the stationary inner walls of the hole in the stationary plate to predict the thrust force and torque generated at the interface during interference friction welding process. The yield stress of the tube and plate material has been used to represent the contact pressure, p. The temperature dependent yield stress of the Al 6061 material obtained from [33] has been used to model the effect of heat generation at the interface that causes the change in measured thrust force and torque values.

The thrust force based on coulomb's friction model for the interference friction welding process can be expressed as,

$$F = 2\pi\mu_a prt \tag{10}$$

The torque at the interface can be expressed as,

$$T = 2\pi\mu_t pr^2 t \tag{11}$$

The contact pressure at the interface can be related to shear yield strength of the material as proposed by Feng et. al. [34] based on the Coulomb's friction law by the equation below,

$$p = \frac{\tau_y}{\mu_t} \tag{12}$$

For equation (10), (11) and (12), p is the contact pressure at the interface which has been expressed in terms of the temperature dependent yield strength of the material. r is the radial distance of the interface from the central axis, t is the thickness of the stationary plate with the drilled hole, μ_t and $\mu_a$are the respective coefficient of friction values along the rotational direction and the axial direction. Since the tube rotates at a high spindle speed of the order of 2500 rpm as compared to the value of feed rate of 8.466 mm/s, the value of rotational coefficient of friction will be much higher as compared to the value of the coefficient of friction along the axial direction.

Temperature (°C)	Yield strength of the Al 6061-T6 (MPa)
37.8	274
93.3	265
149	248
204	219
260	160
316	66.2
371	34.5
427	17.9

Table 8 Temperature-dependent material yield strength of Al 6061-T6 [33]

Using the values of the temperature dependent yield strength of the material listed in Table 8, the analytical values of the peak thrust force and torque as a function of temperature can be predicted using the model presented in equation (10) and equation (11) respectively. Based on the literature review of friction welding processes, the coefficient of friction in the rotational direction can be taken as 2 whereas the coefficient of friction along the axial tube feed direction can be taken as 0.8.

$$\frac{F_t}{\mu_t} = \frac{F_a}{\mu_a} \tag{13}$$

Based on the Coulomb's friction law, the tangential force and the axial force can be equated as shown in equation (13), as the normal force acting to the surface will be the same for the relative motion between the tube and walls of the cylindrical hole in axial and tangential direction.

The predicted values of peak thrust force and torque using the proposed analytical model have been tabulated in Table 9.

Temperature (°C)	Thrust force (N)	Torque (Nm)	Tangential force (N)
37.8	8748.773	138.886	21871.934
93.3	8461.405	134.324	21153.513
149	7918.598	125.707	19796.495
204	6992.633	111.008	17481.583
260	5108.773	81.101	12771.932
316	2113.754	33.555	5284.387
371	1101.579	17.487	2753.948
427	571.543	9.073	1428.859

Table 9 Predicted analytical values of the peak thrust force (N) and torque (Nm)

The values of peak torque, tangential force obtained from the torque values (by dividing torque values by the radial distance of the interface from the central axis) and axial thrust force from the experimental observations for spindle speed 2500 rpm , feed rate 8.46 mm/s, penetration depth of 15 mm have been tabulated below in Table 10.

On comparing the analytical and experimental values of peak axial thrust force from Table 9 and Table 10, it is clear that the axial thrust force is highly over predicted by the analytical model if the change in the material properties at the interface because of heat generation is not considered.

Axial thrust force values (N)	Torque values (Nm)	Tangential force (N)
956.873	12.163	1915.456
1057.187	16.180	2548.152
974.164	13.936	2194.662
997.122	16.379	2579.373

Table 10 Torque and axial thrust force for experimental observations for spindle speed 2500 rpm, feed rate 8.46 mm/s, penetration depth 15 mm

Meaning thereby, the analytical thrust force predicted close to the room temperature is 8 to 9 times the actual axial thrust force observed from the experimental values. Similarly, the torque generated at the interface is over predicted by 8 to 10 times if the reduction in the yield strength of the material due to heat generation at the interface is not considered. Furthermore, on considering the effect of heat generation at the interface with reduction in yield strength of the material at higher temperatures, the analytical model fairly predicts the peak thrust force and torque generated at the interface. From the literature review, it was known that the temperature at the interface for friction welding processes is in the range of 350 to 450 ° C [6, 34]. To estimate the actual heat generation at the interface due to frictional heating and plastic deformation at different spindle speeds, the equations (6), (7) and (8) proposed earlier in this section were used and the obtained values have been tabulated in Table 11.

Spindle speed (rpm)	Angular velocity (rad/s)	$Q_{FRICTIONAL}$ (W)	$Q_{PLASTIC}$ (W)	Q total (W)
1250	130.945	1144.962	572.481	1717.443
1500	157.135	2747.909	686.977	3434.886
2000	209.513	3663.879	915.969	4579.848
2500	261.891	4579.848	1144.962	5724.811
3000	314.270	5495.818	1373.954	6869.773

Table 11 Analytical heat generation rates at different spindle speeds

However, for frictional heat generation at the tube-plate interface, 100% of the dissipated energy caused by friction is assumed to be converted to heat. Based on the heat generation rate an estimate of temperature at the interface can be made with simplifying assumptions. A common heat partition model based on the ratio of thermal conductivity

of the tube and plate material used in several research works including the study by Miller et. al. [17] can be applied to determine the heat partition at the tube-plate interface.

The ratio of the heat partition into the tube material, r_{tube} can be expressed as,

$$r_{tube} = \frac{k_{tube}}{k_{tube}+k_{plate}} \tag{14}$$

where, k_{tube} is the thermal conductivity of tube material,

k_{plate} is the thermal conductivity of plate material

Since, the tube and the plate material is the same in this study, the ratio of the heat partition, r_{tube} will be 0.5.

In order to estimate the temperature at particular spindle speed of 2500 rpm, it can be assumed that 50% of the corresponding total heat generated flows through the material of the tube.

The generalized heat diffusion equation in cylindrical coordinates as expressed in equation (1) can be simplified by assuming a steady state process with a constant heat flow through the thickness of the tube with no internal heat generation. The equation reduces to,

$$\frac{1}{r}\frac{\partial}{\partial r}\left(kr\frac{\partial T}{\partial r}\right) = 0 \tag{15}$$

where, k is thermal conductivity treated as a variable in the general equation is a constant value for the scope of this study, dT is the temperature gradient across the tube wall surfaces, r is the distance of the interface from the tube central axis. The physical significance of this result becomes evident when considered with the appropriate form of the Fourier's law.

The standard expression for the rate of conduction heat flow derived in reference material [36] for the heat flow through the cylinder,

$$Q_r = \frac{2\pi Lk(T_{s1} - T_{s2})}{\ln(\frac{r_2}{r_1})} \quad (16)$$

where, L= effective length of the tube

k= thermal conductivity of tube material

T_{s1}= Tube outer wall temperature

T_{s2}= Tube inner wall temperature

r_2 = Tube outer radius

r_1 = Tube inner radius

This model assumes the conduction heat transfer rate Q_r to be constant in the radial direction. In order to obtain an estimate of outer wall temperature of the tube for the given heat flow through the tube, equation 16 was used. The effective length of the tube was selected to be 2 mm as the actual interaction at a given instant between the mating surfaces occurs for only that fraction of length of the tube. It was assumed that the heat flow occurs in the radial direction only as the actual length of tube is much more than the thickness of the tube. Thermal conductivity of Al 6061 tube was taken to be 237 W/m/k. The inner wall temperature of the hollow tube was assumed to be at ambient temperature of 298 K. The outer and inner radius of the tube were taken as 6.35 mm and 4.24 mm respectively. The estimates of the calculated outer wall temperature of the tube for the given amount of heat flow through the material because of heat generation at the interface at difference spindle speeds is listed in Table 12.

Spindle speed (rpm)	Angular velocity (rad/s)	Q tube (W)	T_{S1} (°C)
1250	130.945	858.721	142.763
1500	157.135	1717.443	260.677
2000	209.513	2289.924	339.286
2500	261.891	2862.405	417.895
3000	314.270	3434.886	496.504

Table 12 Analytical temperature estimates at different spindle speeds

Furthermore, an iterative approach was used to obtain the accurate prediction of the temperature. The second iteration was computed with material properties at 418 °C which was the temperature computed at 2500 rpm. The temperature computed for material properties at 418 °C over-predicted the heat generation as the temperature computed for the 2nd iteration was 259 °C.

Further, the material properties at 400 °C were adopted as input to the heat transfer model and the temperature prediction was 319 °C. The procedure for repeated and convergence of the input and output temperature was achieved. Table 13 lists iterations for the input temperatures for material properties and the temperature predicted by the heat transfer model.

Input temperature (°C)	Yield strength of the material (Pa)	Predicted temperatures (°C)
418	20567900	258.730
400	25903600	318.950
390	28867900	352.760
385	30350000	370.560
380	31832100	387.560
382	31239285	380.740

Table 13 Iterative approach for the prediction of the temperature at the interface

Table 14 presents the comparison of the average of the experimental axial thrust force and the torque values at 2500 rpm with the values computed by the analytical model at a temperature 382 °C.

Average experimental thrust force (N)	Average experimental torque (Nm)	Analytical thrust force (N)	Analytical torque (Nm)
996.336	14.664	997.465	15.834

Table 14 Comparison of the experimental and analytical thrust force and torque

Hence, considering the yield strength of the material at a temperature range of 370-400°C by interpolating the values, it can be observed from the values that the predicted peak axial thrust force and the torque /tangential force generated at the interface comes out to be within 10% of the average of the actually measured experimental values.

6. CONCLUSIONS AND FUTURE WORK

This experimental study investigated the interference friction welding process that can be employed to join a tube and a plate. The heat generation required to obtain the solid state joint due to frictional sliding and the plastic deformation was observed to be strongly influenced by the process parameters. The torque generated at the interface and the reaction force offered by the plate material was used as an indicator of the change in the material properties with heat generation. Hence, a parametric study was performed to evaluate the trend in the reaction force and resistive torque at the interface. Furthermore, the joint quality was evaluated with a microscopic examination and a shear test. Similar tests were performed for the joints formed from the shrink fitting process that is widely used to join tubes and plates. This section will summarize the observations that have been noted to provide a better understanding of interference friction welding process.

6.1 Conclusion

The following conclusions can be drawn as a result of the experimental study on interference friction welding process:

- Experimental trials were performed to investigate the behavior of the thrust force and the torque generated at the interface during the interaction between the rotating tube and the walls of the drilled hole in the stationary plate.
- It was observed that the thrust force increased linearly till the heat generation was not enough to cause the change in the material property. As the tube continued to penetrate, the heat generation caused the material to lose its strength and hence a

corresponding steep drop in the thrust force was observed. However as the tube reached the final penetration depth as defined in the G-code fed to the CNC machine, the rate of reduction in the thrust force was observed to reduce till the machine spindle was turned off by the user. A relieve back effect was observed in the thrust force as the material at the interface cooled down and regained its strength.

- Similarly, the torque generated at the interface increased with an increase in the amount of interaction between the rotating tube and the plate, as the tube continued to penetrate. A steep drop in the torque was observed as the material got softer similar to the trend of the axial thrust force. It was consistently observed for all the experimental trials that the peak torque value was attained only after the tube crossed the entire thickness of the stationary plate and the thrust force value started to drop.
- Further it was observed that, as the machine spindle was stopped, the torque values dropped to zero for the trails where the material at the interface was softened due to heat generation and there was no resistance offered by the material to sudden stoppage of the machine spindle. Whereas, for the experimental trials where the machine spindle was stopped before sufficient heat generation, a resistance from the material to sudden stoppage of the machine spindle was observed with a non-zero residual value of the torque in the trends. Further, as the spindle was released the residual value of the torque dropped down to zero.

- A parametric study of the process was performed for the spindle speeds ranging from 1250 rpm to 3000 rpm, feed rates ranging from 2.116 mm/s to 8.46 mm/s, and at 3 different amount interference (0.2032 mm, 0.3175 mm and 0.635 mm).
- From the parametric study it was observed that for a predefined penetration of the tube through the 2 mm thick sheet metal plate, the increase in the spindle speed at a constant feed rate and constant amount of interference resulted in the increase in the heat generation rate as it was observed from the reduction in the peak values of the axial thrust force and the torque values. Likewise, with an increase in the feed rate at a constant spindle speed and amount of interference, it was observed that the peak values of thrust force and torque increased due to lower overall heat generation before the tube reached the final penetration depth and the spindle was turned off. Hence, the total heat generation at the interface was a combined effect of the relative motion along the rotational direction governed by the spindle speed and the time period of the interaction process which was governed by the feed rate of the tube.
- The reduction in the amount of interference caused a reduction in overall heat generation, as there was a reduction in the heat generation due to plastic deformation. For lower interference levels of the order of 0.2032 mm, the stresses generated at the interface exceeded the strength of the material as a result of which the material was removed before any plastic deformation could occur.
- Based on the parametric analysis followed by microscopic analysis and shear test results, it was observed that a better control of the heat generation rate at interface

was achieved by effectively controlling the parameters. It was observed that the highest joint strength and the shear load sustained was 63 MPa and 5012 N respectively. The microscopic study revealed that a sound joint was obtained if an optimum required amount of overall heat generation was achieved.

- Microscopic study as discussed in the preceding chapters of this thesis revealed cracks at the interference friction welded joints for lower spindle speeds and lower feed rates. However, excessive displacement of the softened material from the weld area was observed for higher spindle speeds and lower feed rates. Hence, it was concluded that for the given geometrical dimensions of the specimen and fixed amount of penetration of the tube, higher spindle speeds at higher feed rates of the tubes fetched the best results.
- From the proposed analytical model based on existing fundamental relations of the Coulomb's law, the temperature dependent analytical values of the thrust force and the torque complied well with the experimentally measured values. For the given geometry and the range of the experimental parameters, the proposed analytical model for the interference friction welding process predicted the thrust force and torque values within 10 % of the experimentally measured values.

6.2 Future Work

There were several concepts about the process that could not be included in the present scope of study due to time restrictions which have been proposed below:

- As discussed in the preceding sections, the spindle was turn off manually as the tube reached the final penetration depth defined by the user in the G-code. To remove the manual element, the spindle turnoff process can be coupled with the feed of the tube using position sensors by modifications in the CNC machine.
- A comprehensive thermomechanical Finite Element Model can be developed to simulate the process that would include the effect of heat generation in the modeling the temperature effect on the material property that would eventually predict realistic torque and the thrust force values.
- The proposed interference friction welding process can be implemented for creating tube to plate joints for dissimilar materials. A rigorous microstructural analysis can be performed to study the joint interface and the changes in the heat affected zone created by the process.

REFERENCES

1. Mohamed, Hewyda & Washburn, Jesseca. (1975). Mechanism of solid state pressure welding. Weld. J. (Miami); (United States). 54.
2. Tylecote, R. F., The Solid Phase Welding of Metals, St. Martin's Press, 1968, pp. 38, 57, 201.
3. Tylecote, R. F., British Welding Journal, Vol. 1, 117, 1954.
4. McEwan, K. M. B. and Milner, D. R., British Welding Journal, Vol. 9, 406, 1962.
5. S, Senthil Kumar & Narayanan, Syama & Denis Ashok, S. (2013). Acoustic emission–based monitoring approach for Friction Stir Welding of aluminum alloy AA6063-T6 with different tool pin profiles. Proceedings of the Institution of Mechanical Engineers Part B Journal of Engineering Manufacture. 227. 407-416. 10.1177/0954405412472673.
6. Sattari, S., Bisadi, H. & Sajed, M., 2012. Mechanical Properties and Temperature Distributions of Thin Friction Stir Welded Sheets of AA5083. International Journal of Mechanics and Applications, 2(1), pp. 1-6.
7. Keydon Sithole and Veeredhi Vasudeva Rao 2016 IOP Conf. Ser.: Mater. Sci. Eng. 114 012036
8. Ahmed, S., Shubhrant, A., Deep, A. & Saha, P., 2014. Development and Analysis of Butt and Lap welds in Micro Friction Stir Welding (μFSW),. Guwahati, Assam, India, AIMTDR, pp. 563-1 - 563-5.
9. Nishibara, T. & Nagasaka, Y., 2004. Development of Micro-Friction Stir Welding. Metz, France, s.n.

10. Scialpi, A., De Filippis, L. A. C., Cuomob, P. & Di Summa, P., 2008. Micro Friction Stir Welding of 2024-6082 aluminium alloys. Welding International, p. 16–22.
11. Scialpi, A. et al., 2008. Mechanical analysis of ultra-thin Friction Stir Welding joined sheets with dissimilar and similar materials. Materials and Design, p. 928–936.
12. Kanan, L.F., Vicharapu, B., Bueno, A.F.B. et al. Metall and Materi Trans B (2018) 49: 699.
13. Kumar, K.; Kalyan, C.; Kailas, Satish V.; and Srivatsan, Tirumalai S., "An Investigation of Friction During Friction Stir Welding of Metallic Materials" (2009).
14. Zuo, Q K, and A C Nunes. *Mechanics Model of Plug Welding*. NASA – Final Report, *Mechanics Model of Plug Welding*.
15. Kumaran, S. Senthil, et al. “Optimization of Friction Welding of Tube to Tube Plate Using an External Tool.” *Structural and Multidisciplinary Optimization*, vol. 42, no. 3, 2010, pp. 449–457., doi:10.1007/s00158-010-0509-7.
16. Muthukumaran, S., et al. “Interfacial Microstructure and Strength of Friction Welding of Steel Tube to Aluminum Tube Plate Using an External Tool.” *Advanced Materials Research*, vol. 383-390, 2011, pp. 877–881., doi:10.4028/www.scientific.net/amr.383-390.877.

17. Miller, S. F., and Shih, A. J., 2007, "Thermo-Mechanical Finite Element Modeling of the Friction Drilling Process," Journal of Manufacturing Science and Engineering, 129(3).
18. Table 13-4, Machine Elements in Mechanical Design, 6th Edition, Mott, Vavrek & Wang ©2018 | Pearson
19. Biswas, Pankaj & Mandal, Nisith. (2011). Effect of Tool Geometries on Thermal History of FSW of AA1100. Welding Journal. 90. 129s-135s.
20. Buchibabu Vicharapu, Luis Fernando Kanan, Thomas Clarke & Amitava De (2017) An investigation on friction hydro-pillar processing, Science and Technology of Welding and Joining, 22:7, 555-561, DOI: 10.1080/13621718.2016.1274849
21. Nandan, Rituraj & Roy, Gour & Lienert, Tom & Debroy, Tarasankar. (2007). Three-dimensional heat and material flow during Friction Stir Welding of mild steel. Acta Materialia. 55. 883-895. 10.1016/j.actamat.2006.09.009.
22. Deng, Zhi & R. Lovell, Michael & A. Tagavi, Kaveh. (2001). Influence of Material Properties and Forming Velocity on the Interfacial Slip Characteristics of Cross Wedge Rolling. Journal of Manufacturing Science and Engineering-transactions of The Asme - J MANUF SCI ENG. 123. 10.1115/1.1383028.
23. V. Soundararajan, S. Zekovic, and R. Kovacevic, Thermo-mechanical model with adaptive boundary conditions for Friction Stir Welding of Al 6061, International Journal of Machine Tools & Manufacture 45 (2005) 1577-1587.

24. Frigaard, O.; Grong, O.; Midling, O.T. Metallurgical and Materials Transactions A 2001, 32, 1189–1200.
25. Mishra, R.S.; Ma, Z.Y. Materials Science and Engineering 2005, 50, 1–78.
26. Song, M.; Kovacevic, R. International Journal of Machine Tools and Manufacture 2003, 43, 605–615.
27. Chen, C.M.; Kovacevic, R. International Journal of Machine Tools and Manufacture 2003, 43, 1319–1326.
28. H. Schmidt and J. Hattel, A local model for the thermomechanical conditions in Friction Stir Welding, Modelling and Simulation in Materials Science and Engineering 13 (2005) 77-93.
29. Chen, Z.; Thomson, P.F. Wear 1996, 201, 221–232.
30. Duffin, F.D.; Bahrani, A.S. Wear 1973, 26, 53–74.
31. Reid, J.V.; Schey, J.A. Adhesion of copper alloys. Wear 1985, 104, 1–20
32. Y.J. Chao, X. Qi, and W. Tang, Heat Transfer in Friction Stir Welding-Experimental and Numerical Studies, Transactions of the ASME, Journal of Manufacturing Science and Engineering 125 (2003) 138-145.
33. (2002). *Atlas of Stress-Strain Curves (2nd Edition).* ASM International. Retrieved from https://app.knovel.com/hotlink/toc/id:kpASSCE002/atlas-stress-strain-curves/atlas-stress-strain-curves
34. Schneider, J.; Beshears, R.; Nunes, Jr., A.C. Materials Science and Engineering A 2006, 435–436, 297–304.

35. Z. Feng, J.E. Gould, and T.J. Lienert, Heat Flow Model for Friction Stir Welding of Aluminum Alloys, Proceedings of the TMS Fall Meeting – Symposium on Hot Deformation of Aluminum Alloys II, Oct 11-Oct 15 1998, Rosemont, IL, USA, pp. 149-158.

36. T. L. Bergman, A. S. Lavine, F. P. Incropera and D. P. DeWitt, *Fundamentals of Heat and Mass Transfer*, 7th ed., Hoboken, NJ: John Wiley & Sons, 2011.

37. Onlinemetals©,"https://www.onlinemetals.com"

38. Kumaran, S. Senthil, et al. "Suitability of Friction Welding of Tube to Tube Plate Using an External Tool Process for Different Tube Diameters-A Study." *Experimental Techniques*, vol. 37, no. 6, 2011, pp. 8–14., doi:10.1111/j.1747-1567.2011.00765.x.

39. Kumaran, S. Senthil, et al. "Effect of Tube Preparations on Joint Strength in Friction Welding of Tube-to-Tube Plate Using an External Tool Process." *Experimental Techniques*, vol. 37, no. 3, 2011, pp. 24–32., doi:10.1111/j.1747-1567.2010.00700.x.

40. Kumaran, S. Senthil, and A. Daniel Das. "Friction Welding Joints of SA 213 Tube to SA 387 Tube Plate Boiler Grade Materials by Using Clearance and Interference Fit Method." *Materials Today: Proceedings*, vol. 5, no. 2, 2018, pp. 8557–8566., doi:10.1016/j.matpr.2017.11.553.

APPENDIX A

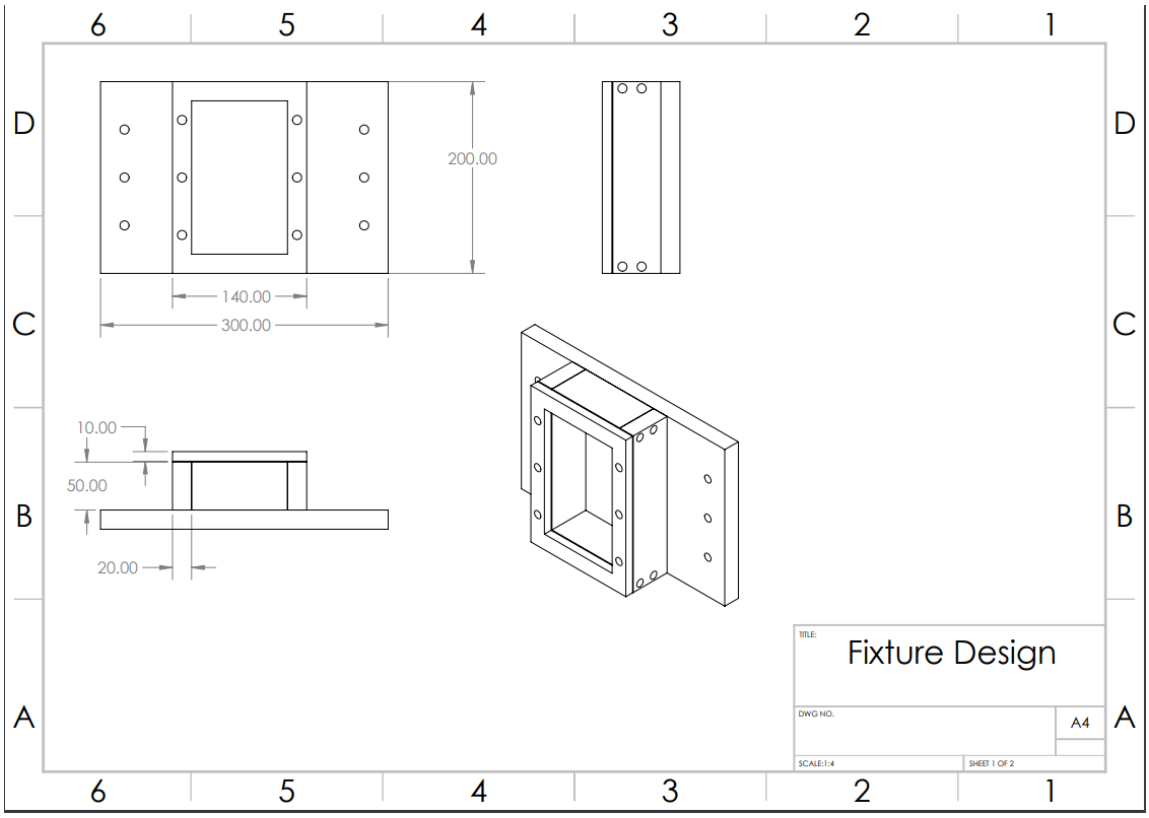

Fixture Design